

Rock mass properties

11.1 Introduction

Reliable estimates of the strength and deformation characteristics of rock masses are required for almost any form of analysis used for the design of slopes, foundations and underground excavations. Hoek and Brown (1980a, 1980b) proposed a method for obtaining estimates of the strength of jointed rock masses, based upon an assessment of the interlocking of rock blocks and the condition of the surfaces between these blocks. This method was modified over the years in order to meet the needs of users who were applying it to problems that were not considered when the original criterion was developed (Hoek 1983, Hoek and Brown 1988). The application of the method to very poor quality rock masses required further changes (Hoek, Wood and Shah 1992) and, eventually, the development of a new classification called the Geological Strength Index (Hoek, Kaiser and Bawden 1995, Hoek 1995, Hoek and Brown 1997). A review of the development of the criterion and of the equations proposed at various stages in this development is given in Hoek and Brown (1997).

This chapter presents the Hoek-Brown criterion in a form that has been found practical in the field and that appears to provide the most reliable set of results for use as input for methods of analysis in current use in rock engineering.

11.2 Generalised Hoek-Brown criterion

The Generalised Hoek-Brown failure criterion for jointed rock masses is defined by:

$$\sigma_1' = \sigma_3' + \sigma_{ci} \left(m_b \frac{\sigma_3'}{\sigma_{ci}} + s \right)^a \quad (11.1)$$

where σ_1' and σ_3' are the maximum and minimum effective stresses at failure,

m_b is the value of the Hoek-Brown constant m for the rock mass,

s and a are constants which depend upon the rock mass characteristics, and

σ_{ci} is the uniaxial compressive strength of the intact rock pieces.

The Mohr envelope, relating normal and shear stresses, can be determined by the method proposed by Hoek and Brown (1980a). In this approach, equation 11.1 is used to generate a series of triaxial test values, simulating full scale field tests, and a

statistical curve fitting process is used to derive an equivalent Mohr envelope defined by the equation:

$$\tau = A\sigma_{ci} \left(\frac{\sigma'_n - \sigma_{tm}}{\sigma_{ci}} \right)^B \quad (11.2)$$

where A and B are material constants

σ'_n is the normal effective stress, and

σ_{tm} is the 'tensile' strength of the rock mass.

This 'tensile' strength, which reflects the interlocking of the rock particles when they are not free to dilate, is given by:

$$\sigma_{tm} = \frac{\sigma_{ci}}{2} \left(m_b - \sqrt{m_b^2 + 4s} \right) \quad (11.3)$$

In order to use the Hoek-Brown criterion for estimating the strength and deformability of jointed rock masses, three 'properties' of the rock mass have to be estimated. These are

1. the uniaxial compressive strength σ_{ci} of the intact rock pieces,
2. the value of the Hoek-Brown constant m_i for these intact rock pieces, and
3. the value of the Geological Strength Index GSI for the rock mass.

11.3 Intact rock properties

For the intact rock pieces that make up the rock mass equation 11.1 simplifies to:

$$\sigma'_1 = \sigma'_3 + \sigma_{ci} \left(m_i \frac{\sigma'_3}{\sigma_{ci}} + 1 \right)^{0.5} \quad (11.4)$$

The relationship between the principal stresses at failure for a given rock is defined by two constants, the uniaxial compressive strength σ_{ci} and a constant m_i . Wherever possible the values of these constants should be determined by statistical analysis of the results of a set of triaxial tests on carefully prepared core samples.

Note that the range of minor principal stress (σ'_3) values over which these tests are carried out is critical in determining reliable values for the two constants. In deriving the original values of σ_{ci} and m_i , Hoek and Brown (1980a) used a range of $0 < \sigma'_3 < 0.5\sigma_{ci}$ and, in order to be consistent, it is essential that the same range be used in any laboratory triaxial tests on intact rock specimens. At least five data points should be included in the analysis.

One type of triaxial cell that can be used for these tests is illustrated in Figure 11.1. This cell, described by Hoek and Franklin (1968), does not require draining between tests and is convenient for the rapid testing of a large number of specimens. More sophisticated cells are available for research purposes but the results obtained from

the cell illustrated in Figure 11.1 are adequate for the rock strength estimates required for estimating σ_{ci} and m_i . This cell has the additional advantage that it can be used in the field when testing materials such as coals, shales and phyllites that are extremely difficult to preserve during transportation and normal specimen preparation for laboratory testing.

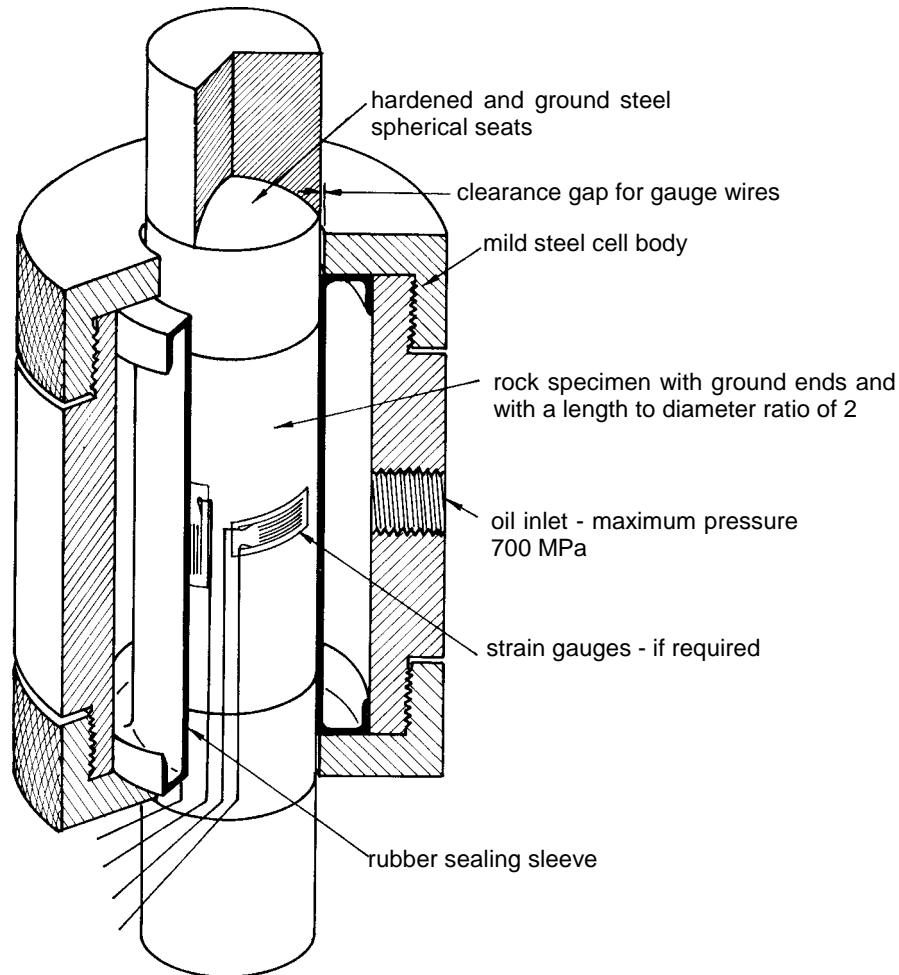


Figure 11.1: Cut-away view of a triaxial cell for testing rock specimens.

Laboratory tests should be carried out at moisture contents as close as possible to those which occur in the field. Many rocks show a significant strength decrease with increasing moisture content and tests on samples, which have been left to dry in a core shed for several months, can give a misleading impression of the intact rock strength.

Once the five or more triaxial test results have been obtained, they can be analysed to determine the uniaxial compressive strength σ_{ci} and the Hoek-Brown constant m_i as described by Hoek and Brown (1980a). In this analysis, equation 11.1 is re-written in the form:

$$y = m\sigma_{ci}x + s\sigma_{ci} \quad (11.5)$$

where $x = \sigma_3'$ and $y = (\sigma_1' - \sigma_3')^2$

For n specimens the uniaxial compressive strength σ_{ci} , the constant m_i and the coefficient of determination r^2 are calculated from:

$$\sigma_{ci}^2 = \frac{\sum y}{n} - \left[\frac{\sum xy - (\sum x \sum y/n)}{\sum x^2 - ((\sum x)^2/n)} \right] \frac{\sum x}{n} \quad (11.6)$$

$$m_i = \frac{1}{\sigma_{ci}} \left[\frac{\sum xy - (\sum x \sum y/n)}{\sum x^2 - ((\sum x)^2/n)} \right] \quad (11.7)$$

$$r^2 = \frac{[\sum xy - (\sum x \sum y/n)]^2}{[\sum x^2 - (\sum x)^2/n][\sum y^2 - (\sum y)^2/n]} \quad (11.8)$$

A spreadsheet for the analysis of triaxial test data is given in Table 11.1. Note that high quality triaxial test data will usually give a coefficient of determination r^2 of greater than 0.9.

When laboratory tests are not possible, Table 11.2 and Table 11.3 can be used to obtain estimates of σ_{ci} and m_i .

Short-term laboratory tests on very hard brittle rocks tend to overestimate the in situ rock mass strength. Laboratory tests and field studies on excellent quality Lac du Bonnet granite, reported by Martin and Chandler (1994), show that the in situ strength of this rock is only about 70% of that measured in the laboratory. This appears to be due to damage resulting from micro-cracking of the rock which initiates and develops critical intensities at lower stress levels in the field than in laboratory tests carried out at higher loading rates on smaller specimens. Hence, when analysing the results of laboratory tests on these types of rocks to estimate the values of σ_{ci} and m_i , it is prudent to reduce the values of the major effective principal stress at failure to 70% of the measured values.

Anisotropic and foliated rocks such as slates, schists and phyllites, the behaviour of which is dominated by closely spaced planes of weakness, cleavage or schistosity, present particular difficulties in the determination of the uniaxial compressive strengths.

Salcedo (1983) has reported the results of a set of directional uniaxial compressive tests on a graphitic phyllite from Venezuela. These results are summarised in Figure 11.2. It will be noted that the uniaxial compressive strength of this material varies by a factor of about 5, depending upon the direction of loading. Evidence of the behaviour of this graphitic phyllite in the field suggests that the rock mass properties are dependent upon the strength parallel to schistosity rather than that normal to it.

Table 11.1: Spreadsheet for the calculation of σ_{ci} and m_i from triaxial test data

Triaxial test data

x	y	xy	xsq	ysq
sig3	sig1			
0	38.3	1466.89	0.0	2151766
5	72.4	4542.76	25.0	20636668
7.5	80.5	5329.00	56.3	28398241
15	115.6	10120.36	225.0	102421687
20	134.3	13064.49	400.0	170680899
47.5	441.1	34523.50	706.3	324289261
sumx	sumy	sumxy	sumxsq	sumysq

Calculation results

Number of tests n = 5
 Uniaxial strength sigci = 37.4
 Hoek-Brown constant mi = 15.50
 Hoek-Brown constant s = 1.00
 Coefficient of determination r2 = 0.997

Cell formulae

$$y = (\text{sig1} - \text{sig3})^2$$

$$\text{sigci} = \text{SQRT}(\text{sumy}/n - (\text{sumxy} - \text{sumx} * \text{sumy}/n) / (\text{sumxsq} - (\text{sumx}^2)/n) * \text{sumx}/n)$$

$$mi = (1/\text{sigci}) * ((\text{sumxy} - \text{sumx} * \text{sumy}/n) / (\text{sumxsq} - (\text{sumx}^2)/n))$$

$$r2 = ((\text{sumxy} - (\text{sumx} * \text{sumy}/n))^2) / ((\text{sumxsq} - (\text{sumx}^2)/n) * (\text{sumysq} - (\text{sumy}^2)/n))$$

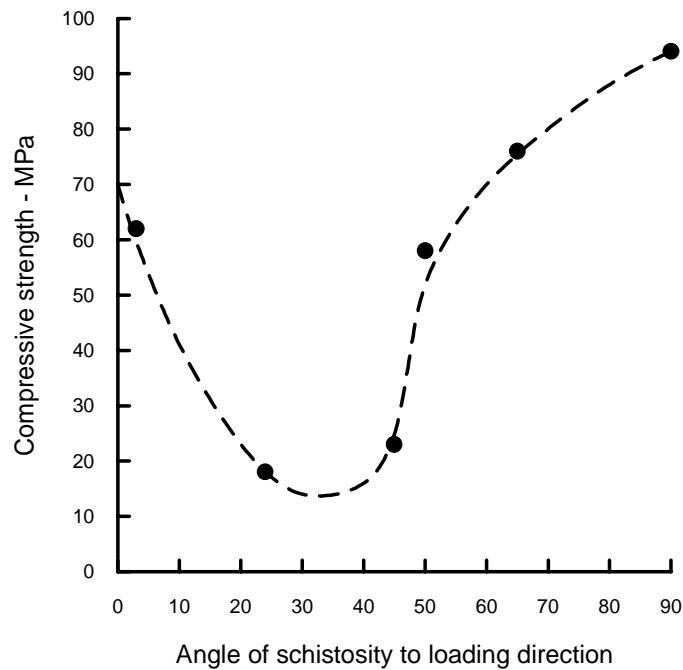


Figure 11.2: Influence of loading direction on the strength of graphitic phyllite tested by Salcedo (1983).

Table 11.2: Field estimates of uniaxial compressive strength.

Grade*	Term	Uniaxial Comp. Strength (MPa)	Point Load Index (MPa)	Field estimate of strength	Examples
R6	Extremely Strong	> 250	>10	Specimen can only be chipped with a geological hammer	Fresh basalt, chert, diabase, gneiss, granite, quartzite
R5	Very strong	100 - 250	4 - 10	Specimen requires many blows of a geological hammer to fracture it	Amphibolite, sandstone, basalt, gabbro, gneiss, granodiorite, limestone, marble, rhyolite, tuff
R4	Strong	50 - 100	2 - 4	Specimen requires more than one blow of a geological hammer to fracture it	Limestone, marble, phyllite, sandstone, schist, shale
R3	Medium strong	25 - 50	1 - 2	Cannot be scraped or peeled with a pocket knife, specimen can be fractured with a single blow from a geological hammer	Claystone, coal, concrete, schist, shale, siltstone
R2	Weak	5 - 25	**	Can be peeled with a pocket knife with difficulty, shallow indentation made by firm blow with point of a geological hammer	Chalk, rocksalt, potash
R1	Very weak	1 - 5	**	Crumbles under firm blows with point of a geological hammer, can be peeled by a pocket knife	Highly weathered or altered rock
R0	Extremely weak	0.25 - 1	**	Indented by thumbnail	Stiff fault gouge

* Grade according to Brown (1981).

** Point load tests on rocks with a uniaxial compressive strength below 25 MPa are likely to yield highly ambiguous results.

Table 11.3: Values of the constant m_i for intact rock, by rock group. Note that values in parenthesis are estimates.

Rock type	Class	Group	Texture			
			Coarse	Medium	Fine	Very fine
SEDIMENTARY	Clastic		Conglomerate (22)	Sandstone 19 —— Greywacke —— (18)	Siltstone 9	Claystone 4
		Organic		—— Chalk —— 7 —— Coal —— (8-21)		
	Non-Clastic	Carbonate	Breccia (20)	Sparitic Limestone (10)	Micritic Limestone 8	
		Chemical		Gypstone 16	Anhydrite 13	
METAMORPHIC	Non Foliated		Marble 9	Hornfels (19)	Quartzite 24	
	Slightly foliated		Migmatite (30)	Amphibolite 25 - 31	Mylonites (6)	
	Foliated*		Gneiss 33	Schists 4 - 8	Phyllites (10)	Slate 9
IGNEOUS	Light		Granite 33		Rhyolite (16)	Obsidian (19)
			Granodiorite (30)		Dacite (17)	
Dark			Diorite (28)		Andesite 19	
			Gabbro 27	Dolerite (19)	Basalt (17)	
		Norite 22				
	Extrusive pyroclastic type		Agglomerate (20)	Breccia (18)	Tuff (15)	

* These values are for intact rock specimens tested normal to bedding or foliation. The value of m_i will be significantly different if failure occurs along a weakness plane.

In deciding upon the value of σ_{ci} for foliated rocks, a decision has to be made on whether to use the highest or the lowest uniaxial compressive strength obtained from

results such as those given in Figure 11.1. Mineral composition, grain size, grade of metamorphism and tectonic history all play a role in determining the characteristics of the rock mass. The author cannot offer any precise guidance on the choice of σ_{ci} but suggest that the maximum value should be used for hard, well interlocked rock masses such as good quality slates. The lowest uniaxial compressive strength should be used for tectonically disturbed, poor quality rock masses such as the graphitic phyllite tested by Salcedo (1983).

Unlike other rocks, coal is organic in origin and therefore has unique constituents and properties. Unless these properties are recognised and allowed for in characterising the coal, the results of any tests will exhibit a large amount of scatter. Medhurst, Brown and Trueman (1995) have shown that, by taking into account the 'brightness' which reflects the composition and the cleating of the coal, it is possible to differentiate between the mechanical characteristics of different coals.

11.4 Influence of sample size

The influence of sample size upon rock strength has been widely discussed in geotechnical literature and it is generally assumed that there is a significant reduction in strength with increasing sample size. Based upon an analysis of published data, Hoek and Brown (1980a) have suggested that the uniaxial compressive strength σ_{cd} of a rock specimen with a diameter of d mm is related to the uniaxial compressive strength σ_{c50} of a 50 mm diameter sample by the following relationship:

$$\sigma_{cd} = \sigma_{c50} \left(\frac{50}{d} \right)^{0.18} \quad (11.9)$$

This relationship, together with the data upon which it was based, is illustrated in Figure 11.3.

The author suggests that the reduction in strength is due to the greater opportunity for failure through and around grains, the 'building blocks' of the intact rock, as more and more of these grains are included in the test sample. Eventually, when a sufficiently large number of grains are included in the sample, the strength reaches a constant value.

Medhurst and Brown (1996) have reported the results of laboratory triaxial tests on samples of 61, 101, 146 and 300 mm diameter samples of a highly cleated mid-brightness coal from the Moura mine in Australia. The results of these tests are summarised in Table 11.4 and Figure 11.4.

The results obtained by Medhurst and Brown show a significant decrease in strength with increasing sample size. This is attributed to the effects of cleat spacing. For this coal, the persistent cleats are spaced at 0.3 to 1.0 m while non-persistent cleats within vitrain bands and individual lithotypes define blocks of 1 cm or less. This cleating results in a 'critical' sample size of about 1 m above which the strength remains constant.

It is reasonable to extend this argument further and to suggest that, when dealing with large scale rock masses, the strength will reach a constant value when the size of individual rock pieces is sufficiently small in relation to the overall size of the

structure being considered. This suggestion is embodied in Figure 11.5 which shows the transition from an isotropic intact rock specimen, through a highly anisotropic rock mass in which failure is controlled by one or two discontinuities, to an isotropic heavily jointed rock mass.

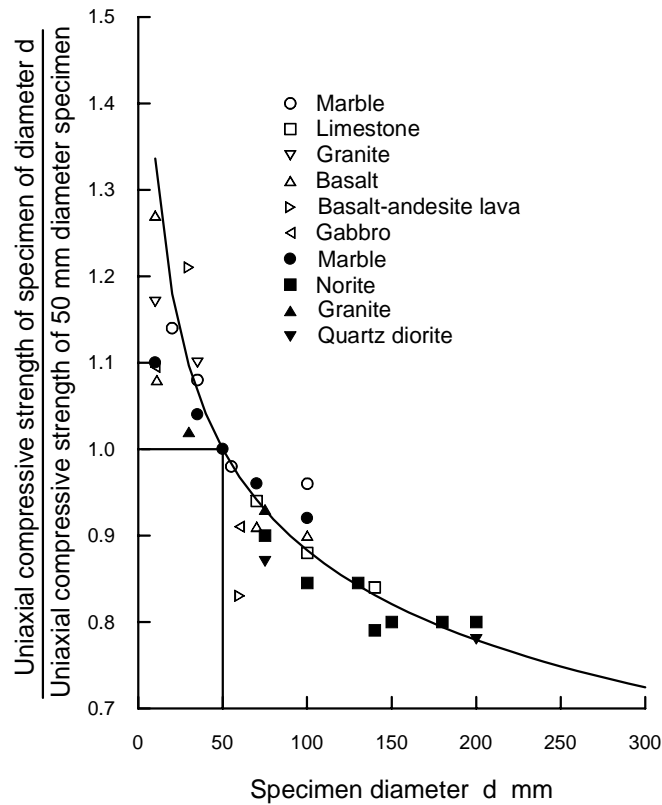


Figure 11.3 Influence of specimen size on the strength of intact rock. After Hoek and Brown (1980a).

Table 11.4 Peak strength of Moura DU coal in terms of the parameters contained in equation (11.1) based upon a value of $\sigma_{ci} = 32.7$ MPa.

Dia.(mm)	m_b	s	a
61	19.4	1.0	0.5
101	13.3	0.555	0.5
146	10.0	0.236	0.5
300	5.7	0.184	0.6
mass	2.6	0.052	0.65

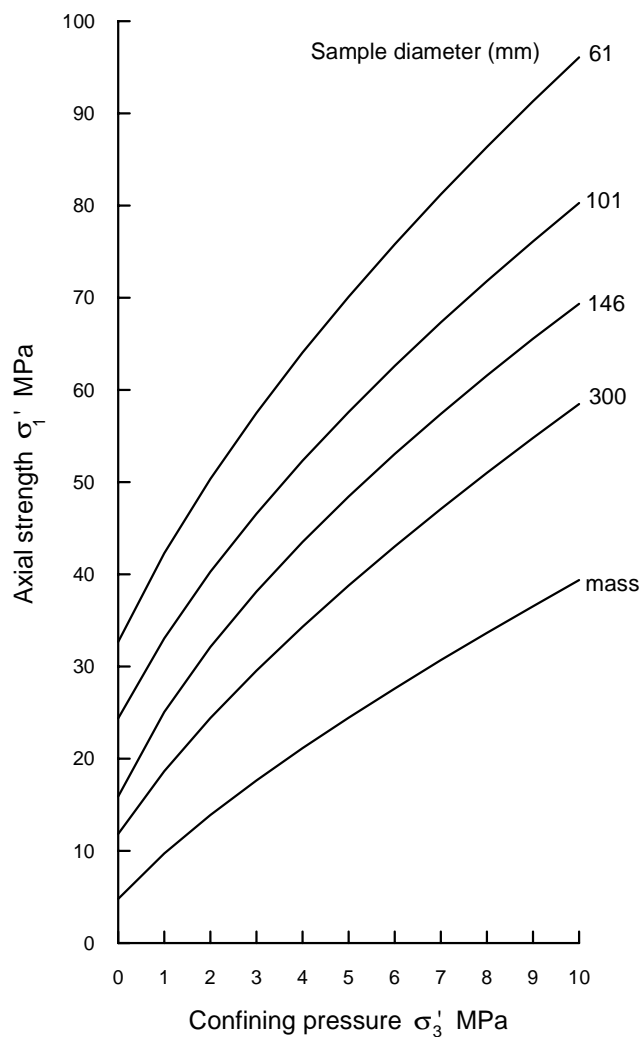


Figure 11.4 Peak strength for Australian Moura coal.
After Medhurst and Brown (1996).

The Hoek-Brown failure criterion, which assumes isotropic rock and rock mass behaviour, should only be applied to those rock masses in which there are a sufficient number of closely spaced discontinuities, with similar surface characteristics, that isotropic behaviour involving failure on discontinuities can be assumed. When the structure being analysed is large and the block size small in comparison, the rock mass can be treated as a Hoek-Brown material.

Where the block size is of the same order as that of the structure being analysed or when one of the discontinuity sets is significantly weaker than the others, the Hoek-Brown criterion should not be used. In these cases, the stability of the structure should be analysed by considering failure mechanisms involving the sliding or rotation of blocks and wedges defined by intersecting structural features.

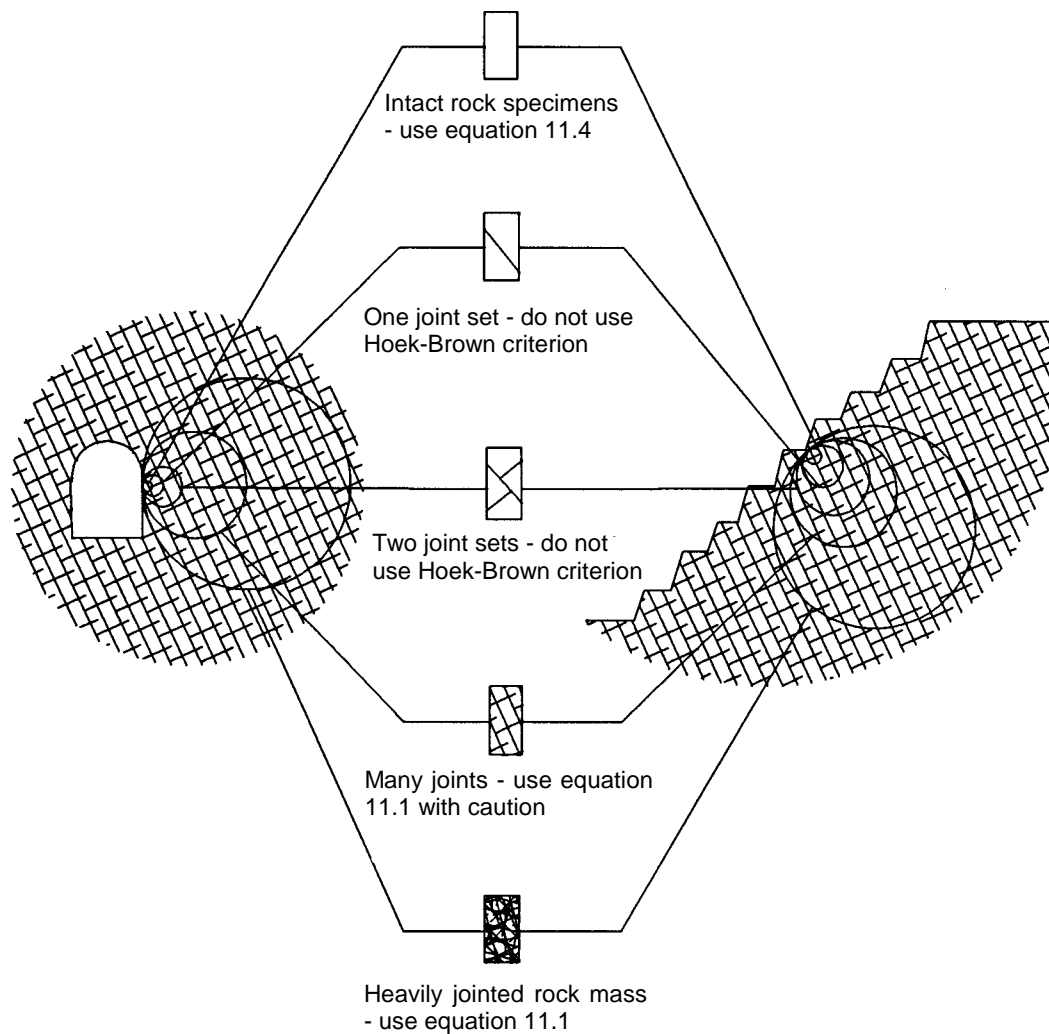


Figure 11.5: Idealised diagram showing the transition from intact to a heavily jointed rock mass with increasing sample size.

11.5 Geological strength Index

The strength of a jointed rock mass depends on the properties of the intact rock pieces and also upon the freedom of these pieces to slide and rotate under different stress conditions. This freedom is controlled by the geometrical shape of the intact rock pieces as well as the condition of the surfaces separating the pieces. Angular rock pieces with clean, rough discontinuity surfaces will result in a much stronger rock mass than one which contains rounded particles surrounded by weathered and altered material.

The Geological Strength Index (GSI), introduced by Hoek (1995) and Hoek, Kaiser and Bawden (1995) provides a system for estimating the reduction in rock mass strength for different geological conditions. This system is presented in Table 11.5 and Table 11.6. Experience has shown that Table 11.5 is sufficient for field

observations since the letter code that identifies each rock mass category can be entered into a field log. Later, these codes can be used to estimate the GSI value from Table 11.6.

Once the Geological Strength Index has been estimated, the parameters that describe the rock mass strength characteristics, are calculated as follows:

$$m_b = m_i \exp\left(\frac{GSI - 100}{28}\right) \quad (11.10)$$

For $GSI > 25$, i.e. rock masses of good to reasonable quality, the original Hoek-Brown criterion is applicable with

$$s = \exp\left(\frac{GSI - 100}{9}\right) \quad (11.11)$$

and

$$a = 0.5 \quad (11.12)$$

For $GSI < 25$, i.e. rock masses of very poor quality, the modified Hoek-Brown criterion applies with

$$s = 0 \quad (11.13)$$

and

$$a = 0.65 - \frac{GSI}{200} \quad (11.14)$$

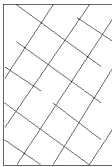
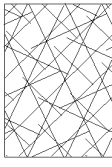


The choice of $GSI = 25$ for the switch between the original and modified criteria is purely arbitrary. It could be argued that a switch at $GSI = 30$ would not introduce a discontinuity in the value of a , but extensive trials have shown that the exact location of this switch has negligible practical significance.

For better quality rock masses ($GSI > 25$), the value of GSI can be estimated directly from the 1976 version of Bieniawski's Rock Mass Rating, with the Groundwater rating set to 10 (dry) and the Adjustment for Joint Orientation set to 0 (very favourable) (Bieniawski 1976). For very poor quality rock masses the value of RMR is very difficult to estimate and the balance between the ratings no longer gives a reliable basis for estimating rock mass strength. Consequently, Bieniawski's RMR classification should not be used for estimating the GSI values for poor quality rock masses.

If the 1989 version of Bieniawski's RMR classification (Bieniawski 1989) is used, then $GSI = RMR_{89}' - 5$ where RMR_{89}' has the Groundwater rating set to 15 and the Adjustment for Joint Orientation set to zero.

One of the practical problems which arises when assessing the value of GSI in the field is related to blast damage. As illustrated in Figure 11.6, there is a considerable difference in the appearance of a rock face which has been excavated by controlled blasting and a face which has been damaged by bulk blasting. Wherever possible, the undamaged face should be used to estimate the value of GSI since the overall aim is to determine the properties of the undisturbed rock mass.

Table 11.5: Characterisation of rock masses on the basis of interlocking and joint alteration¹

<p>ROCK MASS CHARACTERISTICS FOR STRENGTH ESTIMATES</p> <p>Based upon the appearance of the rock, choose the category that you think gives the best description of the 'average' undisturbed in situ conditions. Note that exposed rock faces that have been created by blasting may give a misleading impression of the quality of the underlying rock. Some adjustment for blast damage may be necessary and examination of diamond drill core or of faces created by pre-split or smooth blasting may be helpful in making these adjustments. It is also important to recognize that the Hoek-Brown criterion should only be applied to rock masses where the size of individual blocks is small compared with the size of the excavation under consideration.</p>		<p>SURFACE CONDITIONS</p> <p>VERY GOOD Very rough, fresh unweathered surfaces</p> <p>GOOD Rough, slightly weathered, iron stained surfaces</p> <p>FAIR Smooth, moderately weathered or altered surfaces</p> <p>POOR Slickensided, highly weathered surfaces with compact coatings or fillings of angular fragments</p> <p>VERY POOR Slickensided, highly weathered surfaces with soft clay coatings or fillings</p> <p>DECREASING SURFACE QUALITY ▼</p>				
<p>STRUCTURE</p>		<p>DECREASING INTERLOCKING OF ROCK PIECES ▼</p>				
	<p>BLOCKY - very well interlocked undisturbed rock mass consisting of cubical blocks formed by three orthogonal discontinuity sets</p>	<p>B/VG</p>	<p>B/G</p>	<p>B/F</p>	<p>B/P</p>	<p>B/VP</p>
	<p>VERY BLOCKY - interlocked, partially disturbed rock mass with multifaceted angular blocks formed by four or more discontinuity sets</p>	<p>VB/VG</p>	<p>VB/G</p>	<p>VB/F</p>	<p>VB/P</p>	<p>VB/VP</p>
	<p>BLOCKY/DISTURBED- folded and/or faulted with angular blocks formed by many intersecting discontinuity sets</p>	<p>BD/VG</p>	<p>BD/G</p>	<p>BD/F</p>	<p>BD/P</p>	<p>BD/VP</p>
	<p>DISINTEGRATED - poorly interlocked, heavily broken rock mass with a mixture of angular and rounded rock pieces</p>	<p>D/VG</p>	<p>D/G</p>	<p>D/F</p>	<p>D/P</p>	<p>D/VP</p>

¹ In earlier versions of this table the terms **BLOCKY/SEAMY** and **CRUSHED** were used, following the terminology used by Terzaghi (1946). However, these terms proved to be misleading and they have been replaced, in this table by **BLOCKY/DISTURBED**, which more accurately reflects the increased mobility of a rock mass which has undergone some folding and/or faulting, and **DISINTEGRATED** which encompasses a wider range of particle shapes.

Table 11.6: Estimate of Geological Strength Index GSI based on geological descriptions.

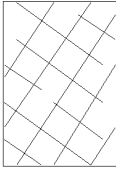
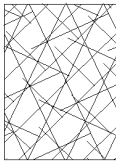

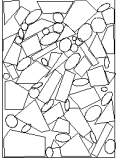
<p>GEOLOGICAL STRENGTH INDEX</p> <p>From the letter codes describing the structure and surface conditions of the rock mass (from Table 4), pick the appropriate box in this chart. Estimate the average value of the Geological Strength Index (GSI) from the contours. Do not attempt to be too precise. Quoting a range of GSI from 36 to 42 is more realistic than stating that GSI = 38.</p>		<p>SURFACE CONDITIONS</p> <p>VERY GOOD Very rough, fresh unweathered surfaces</p> <p>GOOD Rough, slightly weathered, iron stained surfaces</p> <p>FAIR Smooth, moderately weathered or altered surfaces</p> <p>POOR Slickensided, highly weathered surfaces with compact coatings or fillings of angular fragments</p> <p>VERY POOR Slickensided, highly weathered surfaces with soft clay coatings or fillings</p> <p>DECREASING SURFACE QUALITY ▾</p>				
<p>STRUCTURE</p>		<p>DECREASING INTERLOCKING OF ROCK PIECES ▾</p>				
	<p>BLOCKY - very well interlocked undisturbed rock mass consisting of cubical blocks formed by three orthogonal discontinuity sets</p>	80	70			
	<p>VERY BLOCKY - interlocked, partially disturbed rock mass with multifaceted angular blocks formed by four or more discontinuity sets</p>	60	50			
	<p>BLOCKY/DISTURBED- folded and/or faulted with angular blocks formed by many intersecting discontinuity sets</p>	40	30			
	<p>DISINTEGRATED - poorly interlocked, heavily broken rock mass with a mixture of angular and rounded rock pieces</p>	20	10			



Figure 11.6: Comparison between the results achieved using controlled blasting (on the left) and normal bulk blasting for a surface excavation in gneiss.

Where all the visible faces have been damaged by blasting, some attempt should be made to compensate for the lower values of GSI obtained from such faces. In recently blasted faces, new discontinuity surfaces will have been created by the blast and these will give a GSI value that may be as much as 10 points lower than that for the undisturbed rock mass. In other words, severe blast damage can be allowed for by moving up one row in Table 11.5 and Table 11.6.

Where blast damaged faces have been exposed for a number of years, it may also be necessary to step as much as one column to the left in order to allow for surface weathering which will have occurred during this exposure. Hence, for example, a badly blast damaged weathered rock surface which has the appearance of a BLOCKY/DISTURBED and FAIR (BD/F in Table 11.5) rock mass may actually be VERY BLOCKY and GOOD (VB/G) in its unweathered and undisturbed in situ state.

An additional practical question is whether borehole cores can be used to estimate the GSI value behind the visible faces? For reasonable quality rock masses ($GSI > 25$) the best approach is to evaluate the core in terms of Bieniawski's RMR classification and then, as described above, to estimate the GSI value from RMR. For poor quality rock masses ($GSI < 25$), relatively few intact core pieces longer than 100 mm are recovered and it becomes difficult to determine a reliable value for RMR. In these circumstances, the physical appearance of the material recovered in the core should be used as a basis for estimating GSI.

11.6 Mohr-Coulomb parameters

Most geotechnical software is written in terms of the Mohr-Coulomb failure criterion in which the rock mass strength is defined by the cohesive strength c' and the angle of friction ϕ' . The linear relationship between the major and minor principal stresses, σ'_1 and σ'_3 , for the Mohr-Coulomb criterion is

$$\sigma'_1 = \sigma_{cm} + k\sigma'_3 \quad (11.15)$$

where σ_{cm} is the uniaxial compressive strength of the rock mass and k is the slope of the line relating σ'_1 and σ'_3 . The values of ϕ' and c' can be calculated from

$$\sin \phi' = \frac{k-1}{k+1} \quad (11.16)$$

$$c' = \frac{\sigma_{cm}(1 - \sin \phi')}{2 \cos \phi'} \quad (11.17)$$

There is no direct correlation between equation 11.15 and the non-linear Hoek-Brown criterion defined by equation 11.1. Consequently, determination of the values of c' and ϕ' for a rock mass that has been evaluated as a Hoek-Brown material is a difficult problem.

The author believes that the most rigorous approach available, for the original Hoek-Brown criterion, is that developed by Dr J.W. Bray and reported by Hoek (1983). For any point on a surface of concern in an analysis such as a slope stability calculation, the effective normal stress is calculated using an appropriate stress analysis technique. The shear strength developed at that value of effective normal stress is then calculated from the equations given in Hoek and Brown (1997). The difficulty in applying this approach in practice is that most of the geotechnical software currently available provides for constant rather than effective normal stress dependent values of c' and ϕ' .

Having evaluated a large number of possible approaches to this problem, it has been concluded that the most practical solution is to treat the problem as an analysis of a set of full-scale triaxial strength tests. The results of such tests are simulated by using the Hoek-Brown equation 11.1 to generate a series of triaxial test values. Equation 11.15 is then fitted to these test results by linear regression analysis and the values of c' and ϕ' are determined from equations 11.17 and 11.16. The steps required to determine the parameters A, B, c' and ϕ' are given below. A spreadsheet for carrying out this analysis, with a listing of all the cell formulae, is given in Figure 11.7.

The relationship between the normal and shear stresses can be expressed in terms of the corresponding principal effective stresses as suggested by Balmer (1952):

$$\sigma'_n = \sigma'_3 + \frac{\sigma'_1 - \sigma'_3}{\partial \sigma'_1 / \partial \sigma'_3 + 1} \quad (11.18)$$

$$\tau = (\sigma_1' - \sigma_3') \sqrt{\partial \sigma_1' / \partial \sigma_3'} \quad (11.19)$$

For the $GSI > 25$, when $a = 0.5$:

$$\frac{\partial \sigma_1'}{\partial \sigma_3'} = 1 + \frac{m_b \sigma_{ci}}{2(\sigma_1' - \sigma_3')} \quad (11.20)$$

For $GSI < 25$, when $s = 0$:

$$\frac{\partial \sigma_1'}{\partial \sigma_3'} = 1 + am_b^a \left(\frac{\sigma_3'}{\sigma_{ci}} \right)^{a-1} \quad (11.21)$$

The tensile strength of the rock mass is calculated from:

$$\sigma_{tm} = \frac{\sigma_{ci}}{2} \left(m_b - \sqrt{m_b^2 + 4s} \right) \quad (11.22)$$

The equivalent Mohr envelope, defined by equation 11.2, may be written in the form:

$$Y = \log A + BX \quad (11.23)$$

where

$$Y = \log \left(\frac{\tau}{\sigma_{ci}} \right) \quad X = \log \left(\frac{\sigma_n' - \sigma_{tm}}{\sigma_{ci}} \right) \quad (11.24)$$

Using the value of σ_{tm} calculated from equation 11.22 and a range of values of τ and σ_n' calculated from equations 11.19 and 11.18 the values of A and B are determined by linear regression where :

$$B = \frac{\sum XY - (\sum X \sum Y)/T}{\sum X^2 - (\sum X)^2/T} \quad (11.25)$$

$$A = 10^{(\sum Y/T - B(\sum X/T))} \quad (11.26)$$

and T is the total number of data pairs included in the regression analysis.

The most critical step in this process is the selection of the range of σ_3' values. As far as the author is aware, there are no theoretically correct methods for choosing this range and a trial and error method, based upon practical compromise, has been used for selecting the range included in the spreadsheet presented in Figure 11.7.

For a Mohr envelope defined by equation 11.2, the friction angle ϕ_i' for a specified normal stress σ_{ni}' is given by:

$$\phi'_i = \arctan \left(AB \left(\frac{\sigma'_{ni} - \sigma_{tm}}{\sigma_{ci}} \right)^{B-1} \right) \quad (11.27)$$

The corresponding cohesive strength c'_i is given by:

$$c'_i = \tau - \sigma'_{ni} \tan \phi'_i \quad (11.28)$$

and the corresponding uniaxial compressive strength of the rock mass is :

$$\sigma_{cmi} = \frac{2c'_i \cos \phi'_i}{1 - \sin \phi'_i} \quad (11.29)$$

Note that the cohesive strength c'_i given by equation 11.29 is an upper bound value and that it is prudent to reduce this to about 75% of the calculated value for practical applications.

The values of c' and ϕ' obtained from this analysis are very sensitive to the range of values of the minor principal stress σ'_3 used to generate the simulated full-scale triaxial test results. On the basis of trial and error, it has been found that the most consistent results are obtained when 8 equally spaced values of σ'_3 are used in the range $0 < \sigma'_3 < 0.25\sigma_{ci}$.

An example of the results, which are obtained from this analysis, is given in Figure 11.8. Plots of the values of the ratio c'/σ_{ci} and the friction angle ϕ' , for different combinations of GSI and m_i are given in Figure 11.9.

The spreadsheet includes a calculation for a tangent to the Mohr envelope defined by equation 11.2. A normal stress has to be specified in order to calculate this tangent and, in Figure 11.8, this stress has been chosen so that the friction angle ϕ' is the same for both the tangent and the line defined by $c' = 3.3$ MPa and $\phi' = 30.1^\circ$, determined by the linear regression analysis described earlier. The cohesion intercept for the tangent is $c' = 4.1$ MPa which is approximately 25% higher than that obtained by linear regression analysis of the simulated triaxial test data.

Fitting a tangent to the curved Mohr envelope gives an upper bound value for the cohesive intercept c' . It is recommended that this value be reduced by about 25% in order to avoid over-estimation of the rock mass strength.

There is a particular class of problem for which extreme caution should be exercised when applying the approach outlined above. In some rock slope stability problems, the effective normal stress on some parts of the failure surface can be quite low, certainly less than 1 MPa. It will be noted that in the example given in Figure 11.8, for values of σ'_n of less than about 5 MPa, the straight line, constant c' and ϕ' method overestimates the available shear strength of the rock mass by increasingly significant amounts as σ'_n approaches zero. Under such circumstances, it would be prudent to use values of c' and ϕ' based on a tangent to the shear strength curve in the range of σ'_n values applying in practice.

Figure 11.7 Spreadsheet for calculation of Hoek-Brown and equivalent Mohr-Coulomb parameters

Hoek-Brown and equivalent Mohr Coulomb failure criteria

Input:	sigci = 85 MPa	mi = 10	GSI = 45
Output:	mb = 1.40 sigtm = -0.13 MPa k = 3.01 sigcm = 11.36 MPa	s = 0.0022 A = 0.50 phi = 30.12 degrees E = 6913.7 MPa	a = 0.5 B = 0.70 coh = 3.27 MPa
Tangent:	signt = 15.97 MPa	phit = 30.12 degrees	coht = 4.12 MPa

Calculation:

									Sums
sig3	1E-10	3.04	6.07	9.1	12.14	15.18	18.21	21.25	85.00
sig1	4.00	22.48	33.27	42.30	50.40	57.91	64.98	71.74	347.08
ds1ds3	15.89	4.07	3.19	2.80	2.56	2.40	2.27	2.18	35.35
sign	0.24	6.87	12.56	17.85	22.90	27.76	32.50	37.13	157.80
tau	0.94	7.74	11.59	14.62	17.20	19.48	21.54	23.44	116.55
x	-2.36	-1.08	-0.83	-0.67	-0.57	-0.48	-0.42	-0.36	-6.77
y	-1.95	-1.04	-0.87	-0.76	-0.69	-0.64	-0.60	-0.56	-7.11
xy	4.61	1.13	0.71	0.52	0.39	0.31	0.25	0.20	8.12
xsq	5.57	1.17	0.68	0.45	0.32	0.23	0.17	0.13	8.74
sig3sig1	0.00	68.23	202.01	385.23	612.01	878.92	1183.65	1524.51	4855
sig3sq	0.00	9.22	36.86	82.94	147.45	230.39	331.76	451.56	1290
taucalc	0.96	7.48	11.33	14.45	17.18	19.64	21.91	24.04	
sig1sig3fit	11.36	20.51	29.66	38.81	47.96	57.11	66.26	75.42	
signtaufit	3.41	7.26	10.56	13.63	16.55	19.38	22.12	24.81	
tangent	4.25309	8.10321	11.4032	14.4729	17.3991	20.2235	22.9702	25.655	

Cell formulae:

```

mb = mi*EXP((GSI-100)/28)
s = IF(GSI>25,EXP((GSI-100)/9),0)
a = IF(GSI>25,0.5,0.65-GSI/200)
sigtm = 0.5*sigci*(mb-SQRT(mb^2+4*s))
A = acalc = 10^(sumy/8 - bcalc*sumx/8)
B = bcalc = (sumxy - (sumx*sumy)/8)/(sumxsq - (sumx^2)/8)
k = (sumsig3sig1 - (sumsig3*sumsig1)/8)/(sumsig3sq-(sumsig3^2)/8)
phi = ASIN((k-1)/(k+1))*180/PI()
coh = (sigcm*(1-SIN(phi*PI()/180)))/(2*COS(phi*PI()/180))
sigcm = sumsig1/8 - k*sumsig3/8
E = IF(sigci>100,1000*10^((GSI-10)/40),SQRT(sigci/100)*1000*10^((GSI-10)/40))
phit = (ATAN(acalc*bcalc*((signt-sigtm)/sigci)^(bcalc-1)))*180/PI()
coht = acalc*sigci*((signt-sigtm)/sigci)^(bcalc-signt*TAN(phit*PI()/180))
sig3 = Start at 1E-10 (to avoid zero errors) and increment in 7 steps of sigci/28 to 0.25*sigci
sig1 = sig3+sigci*(((mb*sig3)/sigci)+s)^a
ds1ds3 = IF(GSI>25,(1+(mb*sigci)/(2*(sig1-sig3))),1+(a*mb^a)*(sig3/sigci)^(a-1))
sign = sig3+(sig1-sig3)/(1+ds1ds3)
tau = (sign-sig3)*SQRT(ds1ds3)
x = LOG((sign-sigtm)/sigci)
y = LOG(tau/sigci)
xy = x*y          x sq = x^2          sig3sig1= sig3*sig1          sig3sq = sig3^2
taucalc = acalc*sigci*((sign-sigtm)/sigci)^(bcalc)
s3sifit = sigcm+k*sig3
sntaufit = coh+sign*TAN(phi*PI()/180)
tangent = coht+sign*TAN(phit*PI()/180)
    
```

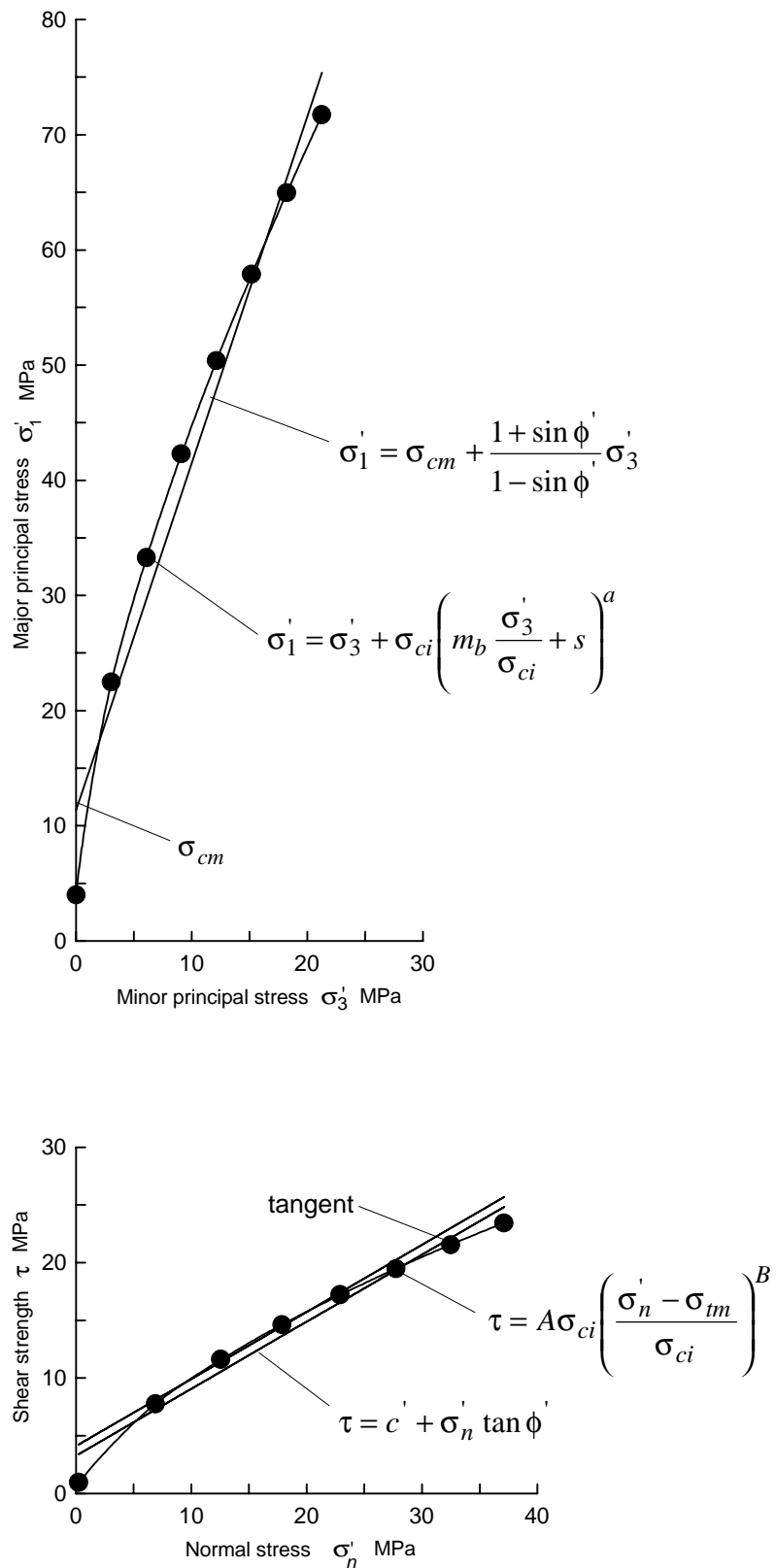
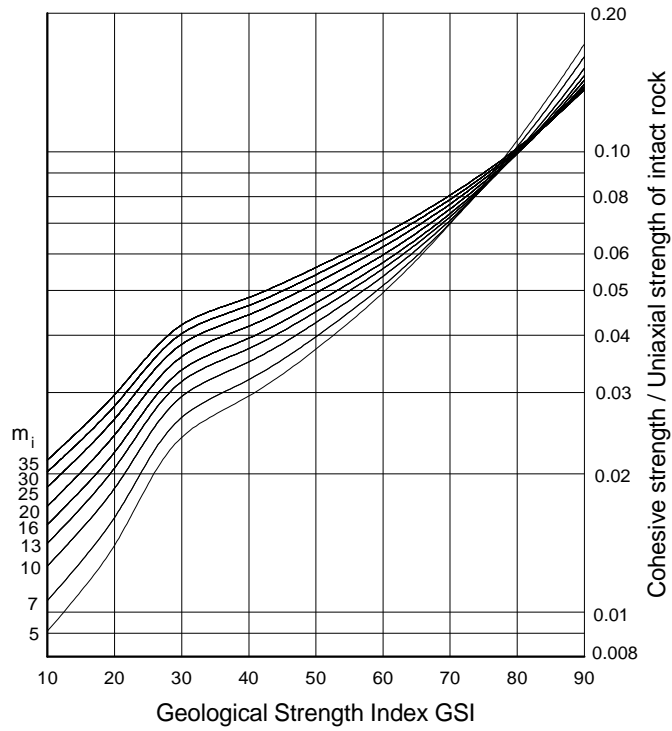
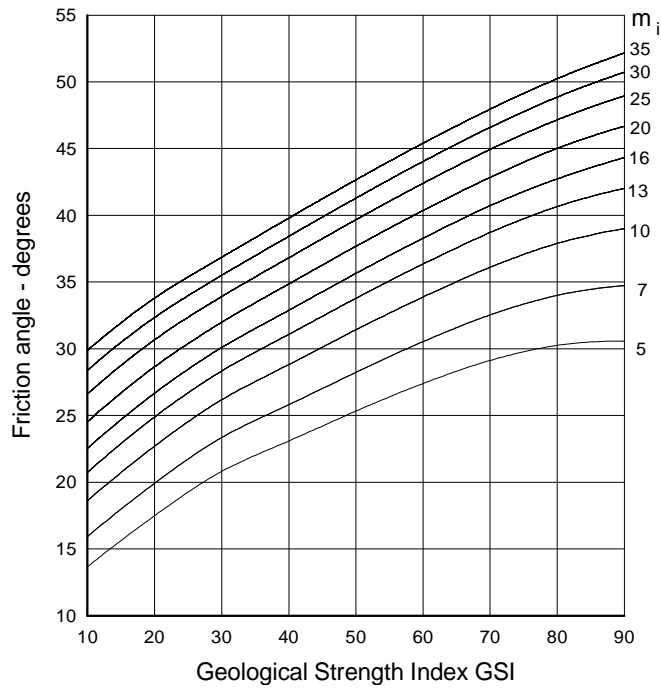


Figure 11.8: Plot of results from simulated full scale triaxial tests on a rock mass defined by a uniaxial compressive strength $\sigma_{ci} = 85$ MPa, a Hoek -Brown constant $m_i = 10$ and a Geological Strength Index $GSI = 45$.



a. Plot of ratio of cohesive strength c' to uniaxial compressive strength σ_{ci} .



b. Plot of friction angle ϕ'

Figure 11.9: Plots of cohesive strength and friction angles for different GSI and m_i values.

11.7 Deformation modulus

Serafim and Pereira (1983) proposed a relationship between the in situ modulus of deformation and Bieniawski's RMR classification. This relationship is based upon back analysis of dam foundation deformations and it has been found to work well for better quality rocks. However, for many of the poor quality rocks it appears to predict deformation modulus values which are too high. Based upon practical observations and back analysis of excavation behaviour in poor quality rock masses, the following modification to Serafim and Pereira's equation is proposed for $\sigma_{ci} < 100$:

$$E_m = \sqrt{\frac{\sigma_{ci}}{100}} 10^{\left(\frac{GSI-10}{40}\right)} \quad (11.30)$$

Note that GSI has been substituted for RMR in this equation and that the modulus E_m is reduced progressively as the value of σ_{ci} falls below 100. This reduction is based upon the reasoning that the deformation of better quality rock masses is controlled by the discontinuities while, for poorer quality rock masses, the deformation of the intact rock pieces contributes to the overall deformation process.

Based upon measured deformations, equation 11.30 appears to work reasonably well in those cases where it has been applied. However, as more field evidence is gathered it may be necessary to modify this relationship.

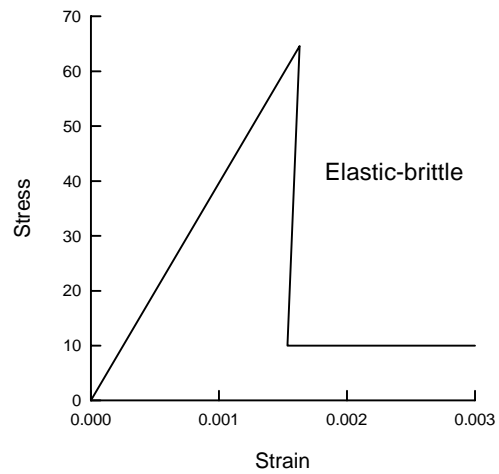
11.8 Post-failure behaviour

When using numerical models to study the progressive failure of rock masses, estimates of the post-peak or post-failure characteristics of the rock mass are required. In some of these models, the Hoek-Brown failure criterion is treated as a yield criterion and the analysis is carried out using plasticity theory (e.g. Pan and Hudson 1988). No definite rules for dealing with this problem can be given but, based upon experience in numerical analysis of a variety of practical problems, the post-failure characteristics illustrated in Figure 11.10 are suggested as a starting point.

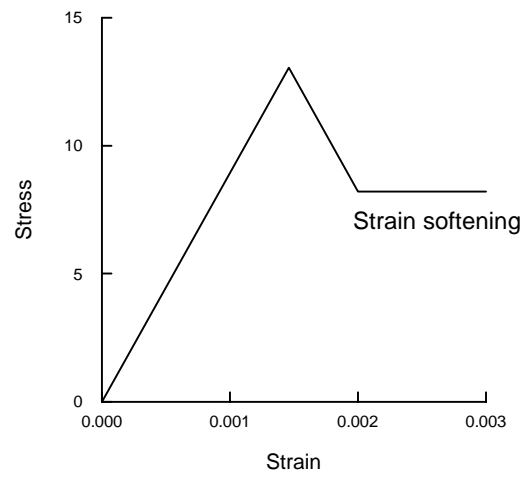
11.8.1 Very good quality hard rock masses

For very good quality hard rock masses, such as massive granites or quartzites, the analysis of spalling around highly stressed openings (Hoek, Kaiser and Bawden 1995) suggests that the rock mass behaves in an elastic brittle manner as shown in Figure 11.10(a). When the strength of the rock mass is exceeded, a sudden strength drop occurs. This is associated with significant dilation of the broken rock pieces. If this broken rock is confined, for example by rock support, then it can be assumed to behave as a rock fill with a friction angle of approximately $\phi' = 38^\circ$ and zero cohesive strength.

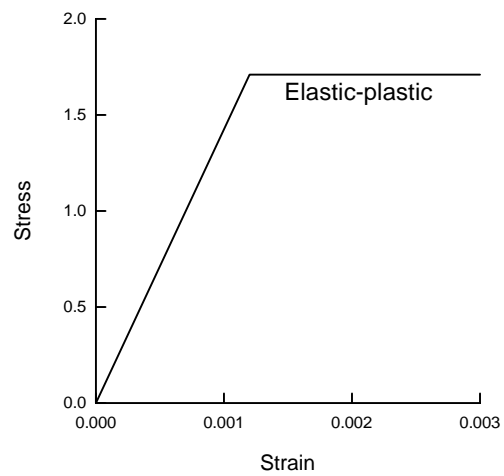
Typical properties for this very good quality hard rock mass may be as shown in Table 11.7. Note that, in some numerical analyses, it may be necessary to assign a very small cohesive strength in order to avoid numerical instability.



(a) Very good quality hard rock mass



(b) Average quality rock mass



(c) Very poor quality soft rock mass

Figure 11.10: Suggested post failure characteristics for different quality rock masses.

Table 11.7: Typical properties for a very good quality hard rock mass

Intact rock strength	σ_{ci}	150 MPa
Hoek-Brown constant	m_i	25
Geological Strength Index	GSI	75
Friction angle	ϕ'	46°
Cohesive strength	c'	13 MPa
Rock mass compressive strength	σ_{cm}	64.8 MPa
Rock mass tensile strength	σ_{tm}	-0.9 MPa
Deformation modulus	E_m	42000 MPa
Poisson's ratio	ν	0.2
Dilation angle	α	$\phi'/4 = 11.5^\circ$
<i>Post-peak characteristics</i>		
Friction angle	ϕ'_f	38°
Cohesive strength	c'_f	0
Deformation modulus	E_{fm}	10000 MPa

11.8.2 Average quality rock mass

In the case of an average quality rock mass it is reasonable to assume that the post-failure characteristics can be estimated by reducing the GSI value from the in situ value to a lower value which characterises the broken rock mass.

The reduction of the rock mass strength from the in situ to the broken state corresponds to the strain softening behaviour illustrated in Figure 11.10(b). In this figure it has been assumed that post failure deformation occurs at a constant stress level, defined by the compressive strength of the broken rock mass. The validity of this assumption is unknown.

Typical properties for this average quality rock mass may be as follows:

Table 10.8: Typical properties for an average rock mass.

Intact rock strength	σ_{ci}	80 MPa
Hoek-Brown constant	m_i	12
Geological Strength Index	GSI	50
Friction angle	ϕ'	33°
Cohesive strength	c'	3.5 MPa
Rock mass compressive strength	σ_{cm}	13 MPa
Rock mass tensile strength	σ_{tm}	-0.15
Deformation modulus	E_m	9000 MPa
Poisson's ratio	ν	0.25
Dilation angle	α	$\phi'/8 = 4^\circ$
<i>Post-peak characteristics</i>		
Broken rock mass strength	σ_{fcm}	8 MPa
Deformation modulus	E_{fm}	5000 MPa

11.8.3 Very poor quality rock mass

Analysis of the progressive failure of very poor quality rock masses surrounding tunnels suggests that the post-failure characteristics of the rock are adequately represented by assuming that it behaves perfectly plastically. This means that it

continues to deform at a constant stress level and that no volume change is associated with this ongoing failure. This type of behaviour is illustrated in Figure 10.10(c). Typical properties for this very poor quality rock mass may be as follows:

Table 11.9: Typical properties for a very poor quality rock mass

Intact rock strength	σ_{ci}	20 MPa
Hoek-Brown constant	m_i	8
Geological Strength Index	GSI	30
Friction angle	ϕ'	24°
Cohesive strength	c'	0.55 MPa
Rock mass compressive strength	σ_{cm}	1.7 MPa
Rock mass tensile strength	σ_{tm}	-0.01 MPa
Deformation modulus	E_m	1400 MPa
Poisson's ratio	ν	0.3
Dilation angle	α	zero
<i>Post-peak characteristics</i>		
Broken rock mass strength	σ_{fcm}	1.7 MPa
Deformation modulus	E_{fm}	1400 MPa

11.9 Reliability of rock mass strength estimates

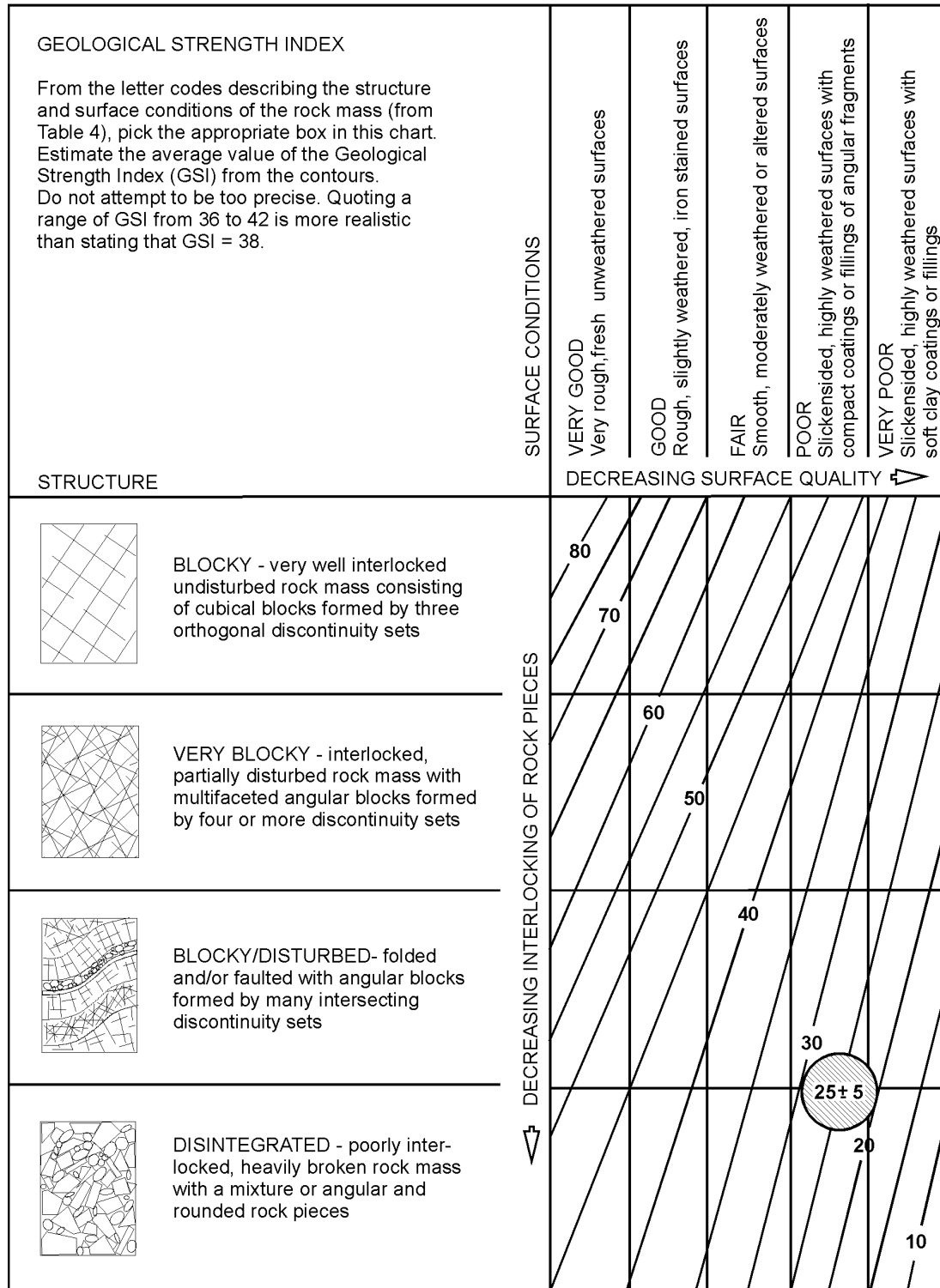
The techniques described in the preceding sections of this chapter can be used to estimate the strength and deformation characteristics of isotropic jointed rock masses. When applying this procedure to rock engineering design problems, most users consider only the 'average' or mean properties. In fact, all of these properties exhibit a distribution about the mean, even under the most ideal conditions, and these distributions can have a significant impact upon the design calculations.

In the text that follows, a slope stability calculation and a tunnel support design calculation are carried out in order to evaluate influence of these distributions. In each case the strength and deformation characteristics of the rock mass are estimated by means of the Hoek-Brown procedure, assuming that the three input parameters are defined by normal distributions.

11.9.1 Input parameters

Figure 11.11 has been used to estimate the value of the value of GSI from field observations of blockiness and discontinuity surface conditions. Included in this figure is a crosshatched circle representing the 90% confidence limits of a GSI value of 25 ± 5 (equivalent to a standard deviation of approximately 2.5). This represents the range of values that an experienced geologist would assign to a rock mass described as BLOCKY/DISTURBED or DISINTEGRATED and POOR. Typically, rocks such as flysch, schist and some phyllites may fall within this range of rock mass descriptions.

Figure 11.11: Estimate of Geological Strength Index GSI based on geological descriptions.



In the author's experience, some geologists go to extraordinary lengths to try to determine an 'exact' value of GSI (or RMR). Geology does not lend itself to such precision and it is simply not realistic to assign a single value. A range of values, such as that illustrated in Figure 11.11 is more appropriate. In fact, in some complex geological environments, the range indicated by the crosshatched circle may be too optimistic.

The two laboratory properties required for the application of the Hoek-Brown criterion are the uniaxial compressive strength of the intact rock (σ_{ci}) and the intact rock material constant m_i . Ideally these two parameters should be determined by triaxial tests on carefully prepared specimens as described by Hoek and Brown (1997).

It is assumed that all three input parameters can be represented by normal distributions as illustrated in Figure 11.12. The standard deviations assigned to these three distributions are based upon the author's experience of geotechnical programs for major civil and mining projects where adequate funds are available for high quality investigations. For preliminary field investigations or 'low budget' projects, it is prudent to assume larger standard deviations for the input parameters.

11.9.2 Output parameters

The values of the friction angle ϕ , the cohesive strength c' , the uniaxial compressive strength of the rock mass σ_{cm} and the deformation modulus E_m of the rock mass were calculated by the procedure described in previous sections of this chapter. The Excel add-on program @RISK² was used for a Monte Carlo analysis in which 1000 calculations were carried out for randomly selected values of the input parameters. The results of these calculations were analysed using the program BESTFIT¹ and it was found that all four output parameters could be adequately described by the normal distributions illustrated in Figure 11.12.

In several trials it was found that the output parameters ϕ , c' and σ_{cm} were always well represented by normal distributions. On the other hand, for *GSI* values of more than 40, the deformation modulus E_m was better represented by a lognormal distribution.

11.9.3 Slope stability calculation

In order to assess the impact of the variation in output parameters, illustrated in Figure 11.12, a calculation of the factor of safety for a homogeneous slope was carried out using Bishop's circular failure analysis in the program SLIDE³. The geometry of the slope and the phreatic surface, the rock mass properties and the critical failure surface for the 'average' properties are shown in Figure 11.13.

² From Palisade Corporation, 31 Decker Road, Newfield, New York 14867, USA.

³ Available from Available from Rocscience Inc., 31 Balsam Avenue, Toronto, Ontario, Canada M4E 3B5, Fax 1 416 698 0908, Phone 1 416 698 8217, Email: software@rocscience.com, Internet <http://www.rocscience.com>.

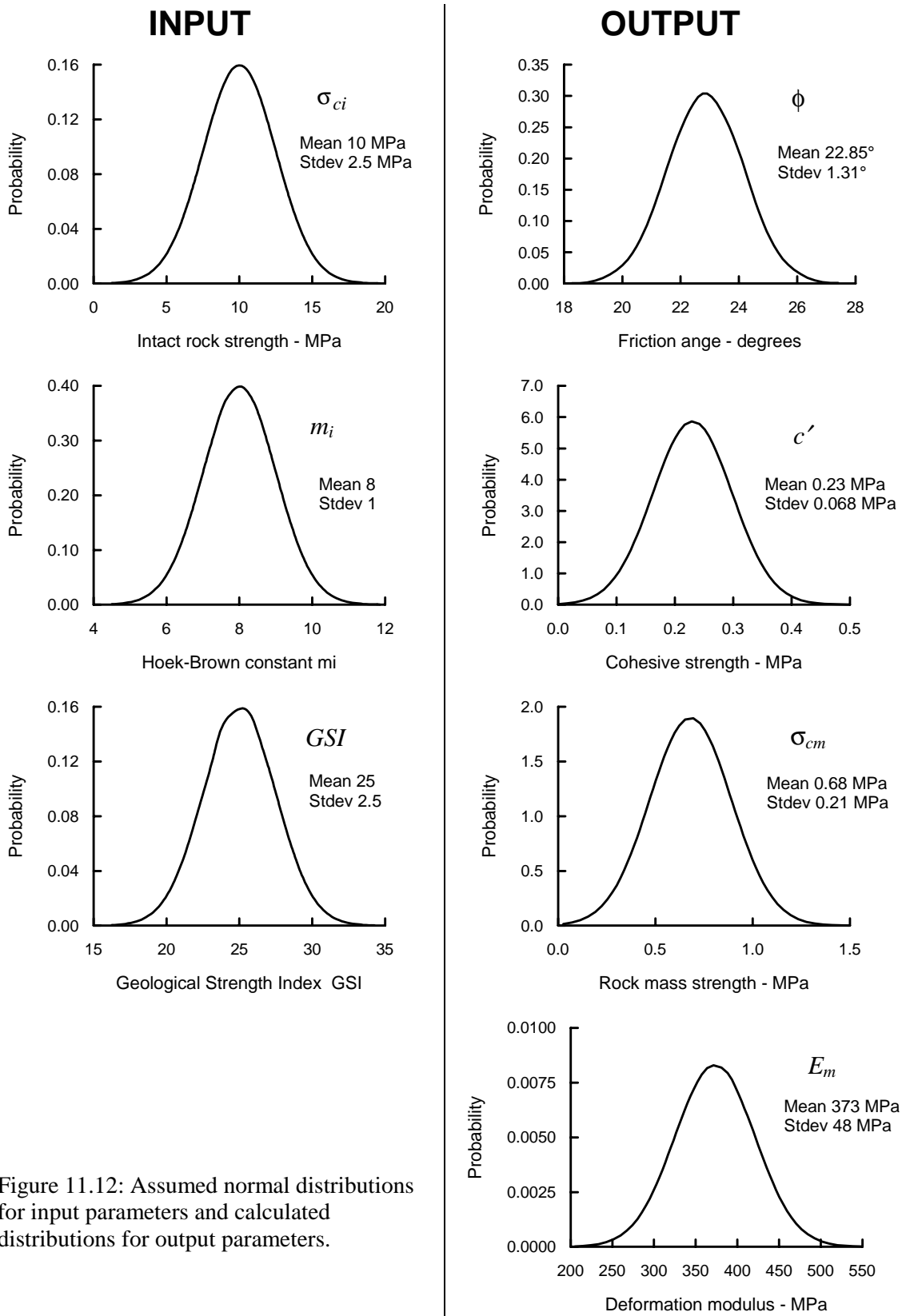


Figure 11.12: Assumed normal distributions for input parameters and calculated distributions for output parameters.

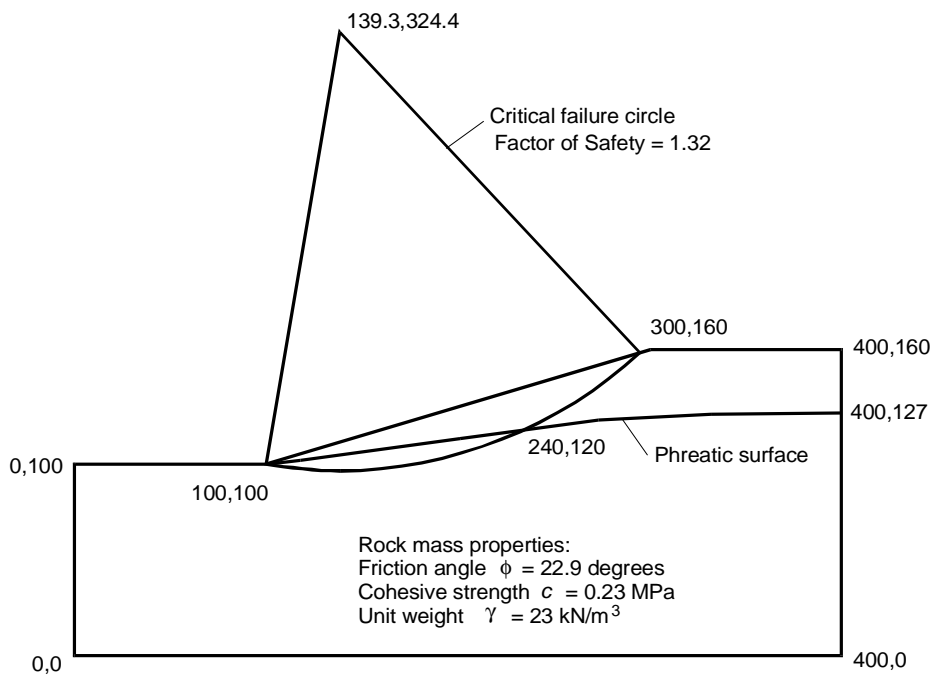


Figure 11.13: Slope and phreatic surface geometry, rock mass properties and critical failure surface for a homogeneous slope.

The distribution of the factor of safety was determined by Rosenbleuth’s Point Estimate method (Rosenbleuth 1976, Harr 1987) in which the two values are chosen at one standard deviation on either side of the mean for each variable. The factor of safety is calculated for every possible combination of point estimates, producing 2^m solutions, where m is the number of variables considered. The mean and standard deviation of the factor of safety are then calculated from these 2^m solutions.

This calculation of the mean and standard deviation is given in Table 11.10. Based upon the fact that the two variables included in this analysis are defined by normal distributions and considering the form of the equations used to calculate the factor of safety, it is reasonable to assume that the factor of safety will be adequately represented by a normal distribution. This distribution is illustrated in Figure 11.13.

Table 11.10: Calculations for Rosenbleuth’s Point Estimate method using \pm one standard deviation.

Case	Friction Angle	Cohesion	Safety Factor	$(SF-SF_i)^2$
ϕ_-, c_-	21.19	0.162	1.215	0.00922
ϕ_+, c_+	24.16	0.298	1.407	0.00922
ϕ_-, c_+	21.19	0.298	1.217	0.00884
ϕ_+, c_-	24.16	0.162	1.406	0.00912
		sums	5.245	0.0364

$$\text{Mean Safety Factor} = \bar{SF} = \frac{1}{n} \sum_{i=1}^n SF_i = 1.31$$

$$\text{Standard deviation} = S^2 = \frac{1}{n-1} \sum_{i=1}^n (\bar{SF} - SF_i)^2 = 0.11$$

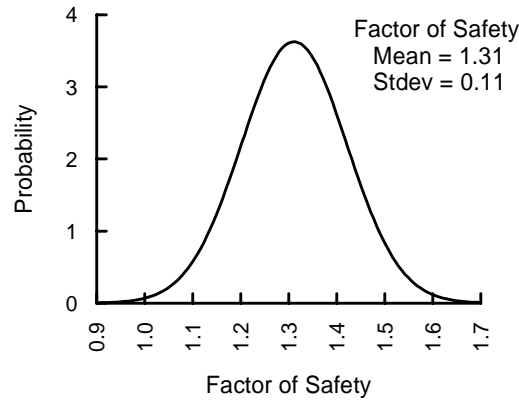


Figure 11.14: Normal distribution of the factor of safety of the slope defined in Figure 11.13.

The mean factor of safety for this slope is 1.3 that is a value frequently used in the design of slopes for open pit mines. It is interesting that the probability of failure, given by the portion of the distribution curve for $SF < 1$, is very small. This suggests that, for a high quality geotechnical investigation such as that assumed in this study, a safety factor of 1.3 is adequate to ensure stability under the assumed conditions.

11.9.4 Tunnel stability calculations

Consider a circular tunnel of radius r_o in a stress field in which the horizontal and vertical stresses are both p_o . If the stresses are high enough, a ‘plastic’ zone of damaged rock of radius r_p surrounds the tunnel. A uniform support pressure p_i is provided around the perimeter of the tunnel. This situation is illustrated in Figure 11.15.

Assuming that the rock mass fails with zero plastic volume change, the critical stress level p_{cr} at which failure initiates is given by :

$$p_{cr} = \frac{2p_o - \sigma_{cm}}{1+k} \quad (11.31)$$

where

$$k = \frac{1 + \sin \phi}{1 - \sin \phi} \quad (11.32)$$

Where the support pressure p_i is less than the critical pressure p_{cr} , the radius r_p of the plastic zone and the inward deformation of the tunnel wall u_{ip} are given by:

$$\frac{r_p}{r_o} = \left[\frac{2(p_o(k-1) + \sigma_{cm})}{(1+k)((k-1)p_i + \sigma_{cm})} \right]^{\frac{1}{(k-1)}} \quad (11.33)$$

$$\frac{u_{ip}}{r_o} = \frac{(1+\nu)}{E} \left[2(1-\nu)(p_o - p_{cr}) \left(\frac{r_p}{r_o} \right)^2 - (1-2\nu)(p_o - p_i) \right] \quad (11.34)$$

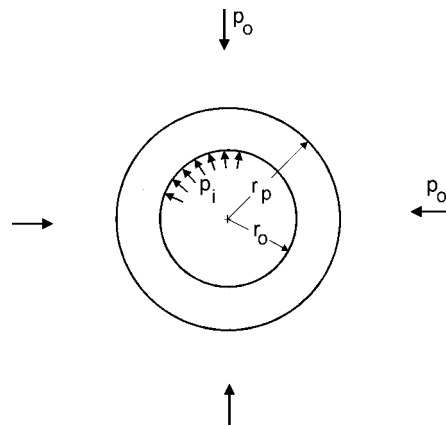


Figure 11.15: Development of a plastic zone around a circular tunnel in a hydrostatic stress field.

In order to study the influence of the variation in the input parameters, a Monte Carlo analysis was performed using the program @RISK in an Excel spreadsheet that had been programmed to perform the analysis defined above. It was assumed that a 5 m diameter tunnel ($r_o = 2.5$ m) was subjected to uniform in situ stress of $p_o = 2.5$ MPa. The rock mass properties were defined by the normal distributions for ϕ , c , σ_{cm} and E defined in Figure 11.12.

This analysis was carried out for a tunnel with no support. A second analysis was performed for a tunnel with a support pressure of $p_i = 0.3$ MPa which is approximately that which can be achieved with a closed ring of 50 mm thick shotcrete with a uniaxial compressive strength of 14 MPa (after 1 day of curing). This would represent the early support that would be achieved by the immediate application of shotcrete behind the advancing face. A third analysis was performed for a support pressure $p_i = 0.8$ MPa. This is approximately the support which can be achieved in this size of tunnel by a 75 mm thick shotcrete lining with a uniaxial compressive strength of 35 MPa (cured for 28 days). The results of these analyses are summarised graphically in Figures 11.16 and 11.17.

Figures 11.16 and 11.17 show that the size of the plastic zone and the tunnel deformation can be represented by lognormal distributions. As would be expected, the mean values for the size of the plastic zone and the magnitude of the sidewall displacements are reduced significantly by the installation of support.

What is surprising is the dramatic reduction in the standard deviations with increasing support pressure. This is because of the strong dependence of the size of the plastic zone upon the difference between the critical pressure p_{cr} and the support pressure p_i . A detailed discussion on this dependence is beyond the scope of this technical note and is the subject of ongoing research by the author.

From the results of the analysis described above it is evident that the installation of a relatively simple support system is very effective in controlling the behaviour of this tunnel. Without support there is an approximate 50% probability of severe instability and possible collapse of the tunnel. A plastic zone diameter of 15 m and a tunnel closure of 50 mm in a 5 m diameter tunnel would certainly cause visible signs of distress. The fact that a relatively thin shotcrete lining can control the size of the

plastic zone and the closure of the tunnel provides confirmation of the effectiveness of support.

A word of warning is required at this point. The example described above is for a 5 m diameter tunnel at a depth of approximately 100 m below surface. For larger tunnels at greater depths, the plastic zone and the displacements can be significantly larger. The demands on the support system may be such that it may be very difficult to support a large tunnel in poor ground at considerable depth below surface.

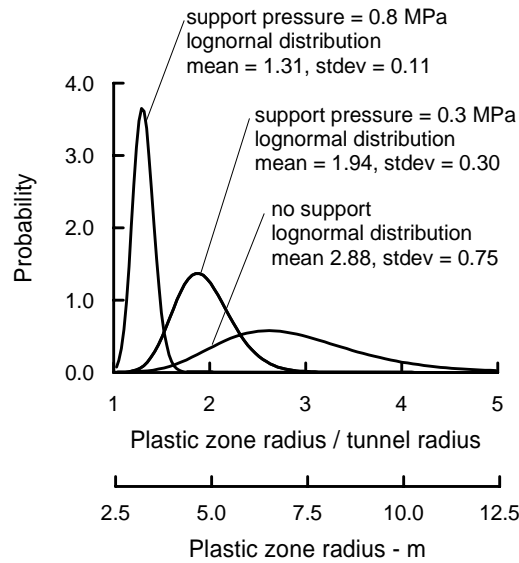


Figure 11.16: Lognormal distributions representing the range of plastic zone radii for different supporting pressures.

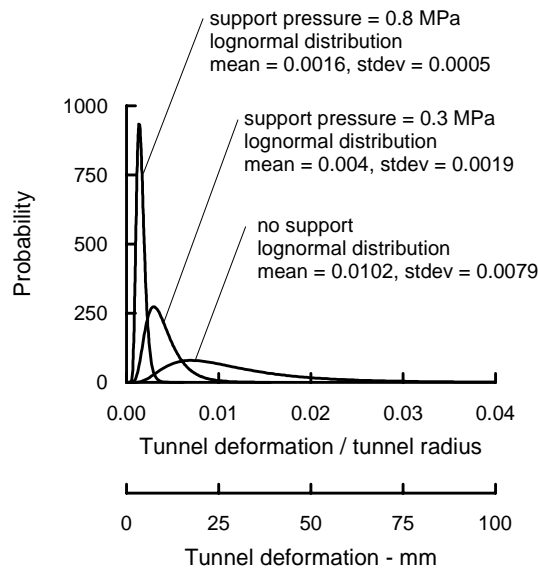


Figure 11.17: Lognormal distributions representing the range of tunnel deformations for different support pressures.

11.9.5 Conclusions

The uncertainty associated with estimating the properties of in situ rock masses has a significant impact on the design of slopes and excavations in rock. The examples that have been explored in this section show that, even when using the ‘best’ estimates currently available, the range of calculated factors of safety or tunnel behaviour are uncomfortably large. These ranges become alarmingly large when poor site investigation techniques and inadequate laboratory procedures are used.

Given the inherent difficulty of assigning reliable numerical values to rock mass characteristics, it is unlikely that ‘accurate’ methods for estimating rock mass properties will be developed in the foreseeable future. Consequently, the user of the Hoek-Brown procedure or of any other equivalent procedure for estimating rock mass properties should not assume that the calculations produce unique reliable numbers. The simple techniques described in this section can be used to explore the possible range of values and the impact of these variations on engineering design.

11.10 Practical examples of rock mass property estimates

The following examples are presented in order to illustrate the range of rock mass properties that can be encountered in the field and to give the reader some insight of how the estimation of rock mass properties was tackled in a number of actual projects.

11.10.1 Massive weak rock

Karzulovic and Diaz (1994) have described the results of a program of triaxial tests on a cemented breccia known as Braden Breccia from the El Teniente mine in Chile. In order to design underground openings in this rock, attempts were made to classify the rock mass in accordance with Bieniawski’s RMR system. However, as illustrated in Figure 11.18, this rock mass has very few discontinuities and so assigning realistic numbers to terms depending upon joint spacing and condition proved to be very difficult. Finally, it was decided to treat the rock mass as a weak but homogeneous ‘almost intact’ rock and to determine its properties by means of triaxial tests on large diameter specimens.

A series of triaxial tests was carried out on 100 mm diameter core samples, illustrated in Figure 11.19. The results of these tests were analysed by means of the regression analysis presented in Section 11.3. Back analysis of the behaviour of underground openings in this rock indicate that the in-situ GSI value is approximately 75. From the spreadsheet presented in Figure 11.7 the following parameters were obtained:

Intact rock strength	σ_{ci}	51 MPa	Friction angle	ϕ'	42°
Hoek-Brown constant	m_i	16.3	Cohesive strength	c'	4.32 MPa
Geological Strength Index	GSI	75	Deformation modulus	E_m	30000 MPa
Hoek-Brown constant	s	0.062			



Figure 11.18: Braden Breccia at El Teniente Mine in Chile. This rock is a cemented breccia with practically no joints. It was dealt with in a manner similar to weak concrete and tests were carried out on 100 mm diameter specimens illustrated in Figure 11.19.



Fig. 11.19. 100 mm diameter by 200 mm long specimens of Braden Breccia from the El Teniente mine in Chile.

11.10.2 Massive strong rock masses

The Rio Grande Pumped Storage Project in Argentina includes a large underground powerhouse and surge control complex and a 6 km long tailrace tunnel. The rock mass surrounding these excavations is a massive gneiss with very few joints. A typical core from this rock mass is illustrated in Figure 11.20. The appearance of the rock at the surface is illustrated in Figure 11.6, which shows a cutting for the dam spillway.



Figure 11.20: Excellent quality core with very few discontinuities from the massive gneiss of the Rio Grande project in Argentina.

Figure 11.21: Top heading of the 12 m span, 18 m high tailrace tunnel for the Rio Grande Pumped Storage Project.



The rock mass can be described as BLOCKY/VERY GOOD and the GSI value, from Table 11.6, is 75. Typical characteristics for the rock mass are as follows:

Intact rock strength	σ_{ci}	110 MPa	Friction angle	ϕ'	43°
Hoek-Brown constant	m_i	17.7	Cohesive strength	c'	9.4 MPa
Geological Strength Index	GSI	75	Rock mass compressive strength	σ_{cm}	43 MPa
Hoek-Brown constant	m_b	7.25	Rock mass tensile strength	σ_{tm}	-0.94 MPa
Hoek-Brown constant	s	0.062	Deformation modulus	E_m	42000 MPa
Constant	a	0.5			

Figure 11.21 illustrates the 8 m high 12 m span top heading for the tailrace tunnel. The final tunnel height of 18 m was achieved by blasting two 5 m benches. The top heading was excavated by full-face drill and blast and, because of the excellent quality of the rock mass and the tight control on blasting quality, most of the top heading did not require any support.

Details of this project are to be found in Moretto et al (1993). Hammett and Hoek (1981) have described the design of the support system for the 25 m span underground powerhouse in which a few structurally controlled wedges were identified and stabilised during excavation.

11.10.3 Average quality rock mass

The partially excavated powerhouse cavern in the Nathpa Jhakri Hydroelectric project in Himachel Pradesh, India is illustrated in Fig. 14. The rock is a jointed quartz mica schist, which has been extensively evaluated by the Geological Survey of India as described by Jalote et al [23]. An average GSI value of 65 was chosen to estimate the rock mass properties which were used for the cavern support design. Additional support, installed on the instructions of the Engineers, was placed in weaker rock zones.

The assumed rock mass properties are as follows:

Intact rock strength	σ_{ci}	30 MPa	Friction angle	ϕ'	40°
Hoek-Brown constant	m_i	15.6	Cohesive strength	c'	2.0 MPa
Geological Strength Index	GS	65	Rock mass compressive strength	σ_{cm}	8.2 MPa
	I				
Hoek-Brown constant	m_b	4.5	Rock mass tensile strength	σ_{tm}	-0.14 MPa
Hoek-Brown constant	s	0.02	Deformation modulus	E_m	13000 MPa
Constant	a	0.5			

Two and three dimensional stress analyses of the nine stages used to excavate the cavern were carried out to determine the extent of potential rock mass failure and to provide guidance in the design of the support system. An isometric view of one of the three dimensional models is given in Figure 11.23.



Figure 11.22: Partially completed 20 m span, 42.5 m high underground powerhouse cavern of the Nathpa Jhakri Hydroelectric Project in Himachel Pradesh, India. The cavern is approximately 300 m below the surface.

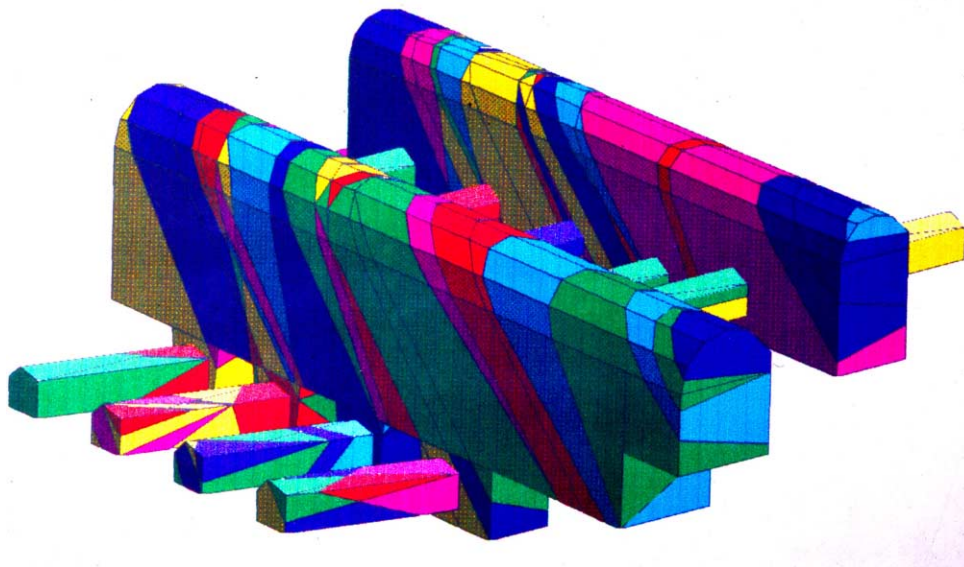


Figure 11.23: Isometric view of the 3DEC⁴ model of the underground powerhouse cavern and transformer gallery of the Nathpa Jhakri Hydroelectric Project, analysed by Dr. B. Dasgupta⁵.

⁴ Available from ITASCA Consulting Group Inc., Thresher Square East, 708 South Third Street, Suite 310, Minneapolis, Minnesota 55415, USA. Fax 1 612 371 4717

⁵ Formerly at the Institute of Rock Mechanics (Kolar), Kolar Gold Fields, Karnataka, now with of Advanced Technology and Engineering Services, Delhi. India.

The support for the powerhouse cavern consists of rockbolts and mesh reinforced shotcrete. Alternating 6 and 8 m long 32 mm diameter bolts on 1 x 1 m and 1.5 x 1.5 m centres are used in the arch. Alternating 9 and 7.5 m long 32 mm diameter bolts are used in the upper and lower sidewalls with alternating 9 and 11 m long 32 mm rockbolts in the centre of the sidewalls, all at a grid spacing of 1.5 m. Shotcrete consists of two 50 mm thick layers of plain shotcrete with an interbedded layer of weldmesh. The support provided by the shotcrete was not included in the support design analysis, which relies upon the rockbolts to provide all the support required.

In the headrace tunnel, some zones of sheared quartz mica schist have been encountered and these have resulted in large displacements as illustrated in Figure 11.24. This is a common problem in hard rock tunnelling where the excavation sequence and support system have been designed for 'average' rock mass conditions. Unless very rapid changes in the length of blast rounds and the installed support are made when an abrupt change to poor rock conditions occurs, for example when a fault is encountered, problems with controlling tunnel deformation can arise.

The only effective way known to the authors for anticipating this type of problem is to keep a probe hole ahead of the advancing face at all times. Typically, a long probe hole is percussion drilled during a maintenance shift and the penetration rate, return water flow and chippings are constantly monitored during drilling. Where significant problems are indicated by this percussion drilling, one or two diamond-drilled holes may be required to investigate these problems in more detail. In some special cases, the use of a pilot tunnel may be more effective in that it permits the ground properties to be defined more accurately than is possible with probe hole drilling. In addition, pilot tunnels allow pre-drainage and pre-reinforcement of the rock ahead of the development of the full excavation profile.

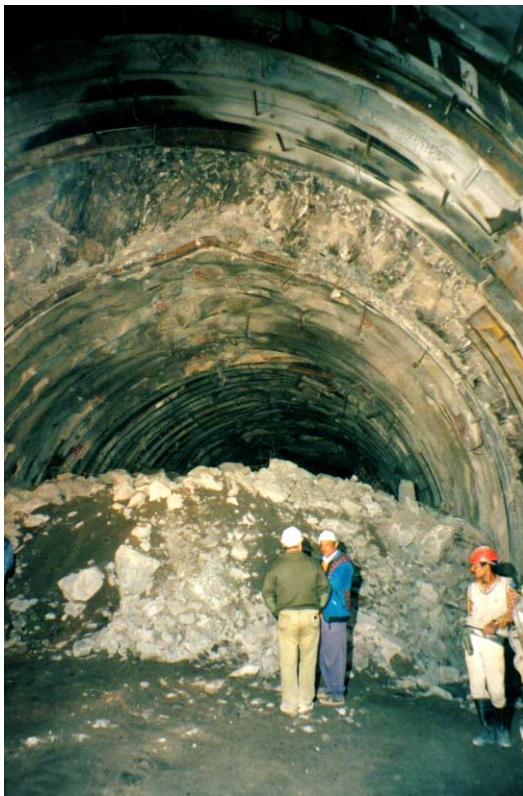


Figure 11.24: Large displacements in the top heading of the headrace tunnel of the Nathpa Jhakri Hydroelectric project. These displacements are the result of deteriorating rock mass quality when tunnelling through a fault zone.

11.10.4 Poor quality rock mass at shallow depth

Kavvadas et al (1996) have described some of the geotechnical issues associated with the construction of 18 km of tunnels and the 21 underground stations of the Athens Metro. These excavations are all shallow with typical depths to tunnel crown of between 15 and 20 m. The principal problem is one of surface subsidence rather than failure of the rock mass surrounding the openings.

The rock mass is locally known as Athenian schist which is a term erroneously used to describe a sequence of Upper Cretaceous flysch-type sediments including thinly bedded clayey and calcareous sandstones, siltstones (greywackes), slates, shales and limestones. During the Eocene, the Athenian schist formations were subjected to intense folding and thrusting. Later extensive faulting caused extensional fracturing and widespread weathering and alteration of the deposits.

The GSI values, estimated from Bieniawski's 1976 RMR classification, modified as recommended by Hoek, Kaiser and Bawden (1995) ranges from about 15 to about 45. The higher values correspond to the intercalated layers of sandstones and limestones, which can be described as BLOCKY/DISTURBED and POOR (Table 11.6). The completely decomposed schist can be described as DISINTEGRATED and VERY POOR and has GSI values ranging from 15 to 20. Rock mass properties for the completely decomposed schist, using a GSI value of 20, are as follows:

Intact rock strength	σ_{ci}	5-10 MPa	Constant	a	0.55
Hoek-Brown constant	m_i	9.6	Friction angle	ϕ'	22.4°
Geological Strength Index	GSI	20	Cohesive strength	c'	0.09-0.18 MPa
Hoek-Brown constant	m_b	0.55	Rock mass strength	σ_{cm}	0.27-0.53 MPa
Hoek-Brown constant	s	0	Deformation modulus	E_m	398-562 MPa

The Academia, Syntagma, Omonia and Olympion stations were constructed using the New Austrian Tunnelling Method twin side drift and central pillar method as illustrated in Figure 11.25. The more conventional top heading and bench method, illustrated in Figure 11.26, was used for the excavation of the Ambelokipi station. These stations are all 16.5 m wide and 12.7 m high. The appearance of the rock mass in one of the Olympion station side drift excavations is illustrated in Figures 11.27 and 11.28.

Numerical analyses of the two excavation methods showed that the twin side drift method resulted in slightly less rock mass failure in the crown of the excavation. However, the final surface displacements induced by the two excavation methods were practically identical.

Maximum vertical displacements of the surface above the centre-line of the Omonia station amounted to 51 mm. Of this, 28 mm occurred during the excavation of the side drifts, 14 mm during the removal of the central pillar and a further 9 mm occurred as a time dependent settlement after completion of the excavation. According to Kavvadas et al (1996), this time dependent settlement is due to the dissipation of excess pore water pressures which were built up during excavation. In the case of the Omonia station, the excavation of recesses towards the eastern end of

the station, after completion of the station excavation, added a further 10 to 12 mm of vertical surface displacement at this end of the station.

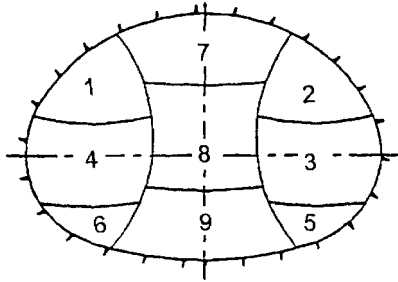


Figure 11.25: Twin side drift and central pillar excavation method. Temporary support consists of double wire mesh reinforced 250 - 300 mm thick shotcrete shells with embedded lattice girders or HEB 160 steel sets at 0.75 - 1 m spacing.

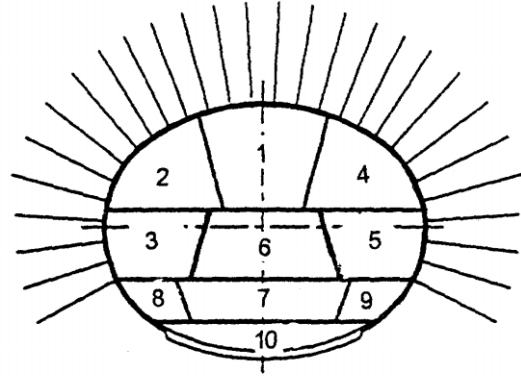


Figure 11.26: Top heading and bench method of excavation. Temporary support consists of a 200 mm thick shotcrete shell with 4 and 6 m long untensioned grouted rockbolts at 1.0 - 1.5 m spacing



Figure 11.27: Side drift in the Athens Metro Olympion station excavation that was excavated by the method illustrated in Figure 11.25. The station has a cover depth of approximately 10 m over the crown.



Figure 11.28: Appearance of the very poor quality Athenian Schist at the face of the side heading illustrated in Figure 11.27.

11.10.5 Poor quality rock mass under high stress

The Yacambú Quibor tunnel in Venezuela is considered to be one of the most difficult tunnels in the world. This 26 km long water supply tunnel through the Andes is being excavated in sandstones and phyllites at depths of up to 1200 m below surface. The graphitic phyllite is a very poor quality rock and gives rise to serious squeezing problems which, without adequate support, result in complete closure of the tunnel. A full-face tunnel-boring machine was completely destroyed in 1979 when trapped by squeezing ground conditions.

At its worst, the graphitic phyllite has an unconfined compressive strength of about 15 MPa and the estimated GSI value is about 24. Typical rock mass properties are as follows:

Intact rock strength	σ_{ci}	15 MPa	Constant	a	0.53
Hoek-Brown constant	m_i	10	Friction angle	ϕ'	24°
Geological Strength Index	GSI	24	Cohesive strength	c'	0.34 MPa
Hoek-Brown constant	m_b	0.66	Rock mass strength	σ_{cm}	1 MPa
Hoek-Brown constant	s	0	Deformation modulus	E_m	870 MPa

Various support methods have been used on this tunnel and only one will be considered here. This was a trial section of tunnel, at a depth of about 600 m, constructed in 1989. The support of the 5.5 m span tunnel was by means of a complete ring of 5 m long, 32 mm diameter untensioned grouted dowels with a 200 mm thick shell of reinforced shotcrete. This support system proved to be very effective but was later abandoned in favour of yielding steel sets (steel sets with sliding joints) because of construction schedule considerations.

Examples of the results of a typical numerical stress analysis of this trial section, carried out using the program PHASE², are given in Figures 11.28 and 11.29. Figure 11.28 shows the extent of failure, with and without support, while Figure 11.29 shows the displacements in the rock mass surrounding the tunnel. Note that the criteria used to judge the effectiveness of the support design are that the zone of failure surrounding the tunnel should lie within the envelope of the rockbolt support, the rockbolts should not be stressed to failure and the displacements should be of reasonable magnitude and should be uniformly distributed around the tunnel. All of these objectives were achieved by the support system described earlier.

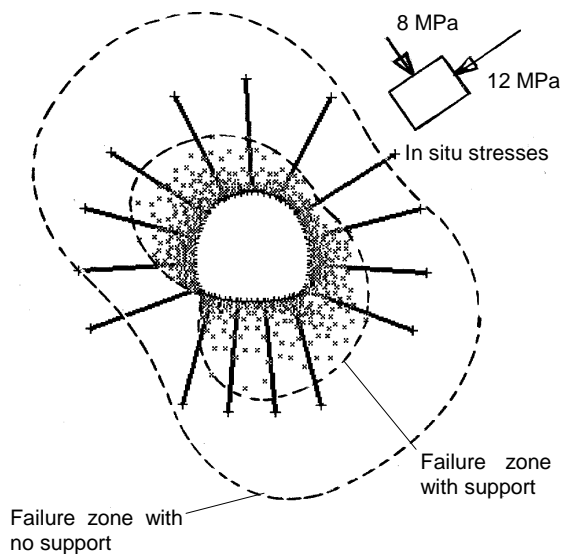


Figure 11.28: Results of a numerical analysis of the failure of the rock mass surrounding the Yacambu-Quibor tunnel when excavated in graphitic phyllite at a depth of about 600 m below surface.

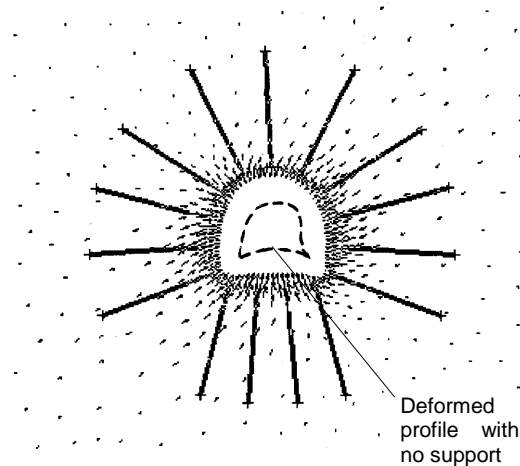


Figure 11.29: Displacements in the rock mass surrounding the Yacambu-Quibor tunnel. The maximum calculated displacement is 258 mm with no support and 106 mm with support.

11.10.6 Slope stability considerations

When dealing with slope stability problems in rock masses, great care has to be taken in attempting to apply the Hoek-Brown failure criterion, particularly for small steep slopes. As illustrated in Figure 11.30, even rock masses that appear to be good candidates for the application of the criterion can suffer shallow structurally controlled failures under the very low stress conditions which exist in such slopes.

As a general rule, when designing slopes in rock, the initial approach should always be to search for potential failures controlled by adverse structural conditions. These may take the form of planar failures on outward dipping features, wedge failures on intersecting features, toppling failures on inward dipping failures or complex failure modes involving all of these processes. Only when the potential for structurally controlled failures has been eliminated should consideration be given to treating the rock mass as an isotropic material as required by the Hoek-Brown failure criterion.



Figure 11.30: Structurally controlled failure in the face of a steep bench in a heavily jointed rock mass.

Figure 11.31 illustrates a case in which the base of a slope failure is defined by an outward dipping fault which does not daylight at the toe of the slope. Circular failure through the poor quality rock mass overlying the fault allows failure of the toe of the slope. Analysis of this problem was carried out by assigning the rock mass at the toe properties that had been determined by application of the Hoek-Brown criterion. A search for the critical failure surface was carried out utilising the program XSTABL⁶ which allows complex failure surfaces to be analysed and which includes facilities for the input of non-linear failure characteristics as defined by equation 11.2.

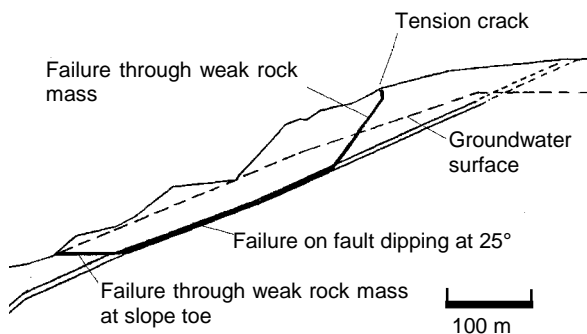


Figure 11.31: Complex slope failure controlled by an outward dipping basal fault and circular failure through the poor quality rock mass overlying the toe of the slope.

⁶ Available from Interactive Software Designs, Inc., 953 N. Cleveland Street, Moscow, Idaho, USA 83843, Fax + 1 208 885 6608